PHILOSOPHICAL TRANSACTIONS OF THE ROYAL SOCIETY A MATHEMATICAL, PHYSICAL & ENGINEERING SCIENCES

# Limit Analysis for Plates: The Exact Solution for a Clamped Square Plate of Isotropic Homogeneous Material Obeying the Square Yield Criterion and Loaded by Uniform Pressure

E. N. Fox

*Phil. Trans. R. Soc. Lond. A* 1974 **277**, 121-155
doi: 10.1098/rsta.1974.0047

# LIMIT ANALYSIS FOR PLATES: THE EXACT SOLUTION FOR A CLAMPED SQUARE PLATE OF ISOTROPIC HOMOGENEOUS MATERIAL OBEYING THE SQUARE YIELD CRITERION AND LOADED BY UNIFORM PRESSURE

By E. N. FOX
*Department of Engineering, University of Cambridge*

(*Communicated by Sir John Baker, F.R.S.* – *Received* 9 *January* 1974)

## CONTENTS



 [Published 29 August 1974

Known exact solutions in limit analysis for rigid–perfectly plastic plates are relatively scarce because of their probable complexity even for simple loading and edge conditions. This complexity is exemplified in the present exact solution for the problem of a uniformly distributed load on a clamped square plate of isotropic homogeneous material obeying the square yield criterion in bending. The solution is extended to cover the case of a uniformly distributed load on a clamped plate of any regular polygonal shape. A comparison of the present exact results and those of Fox (1972) with earlier upper bound solutions is evidence that close upper bounds for the collapse load will normally be obtainable by the use of assumed mechanisms much simpler than the exact mechanism.

## Notation

Excluding subsidiary symbols appearing only briefly where defined in the text, the notation is given below. All moments and shear forces are per unit length along a normal section of the plate.

| | |
|---|---|
| $a$ | radius of inscribed circle for regular polygonal plate |
| $A(\alpha)$, $B(\alpha)$ | arbitrary functions for a parabolic field, equation (22) |
| $f_2(u)$ | arbitrary function for hyperbolic net, equation (18) |
| $F(u)$ | defined by equation (58) |
| $g(u)$ | length PJ, figure 4 |
| $h_1$, $h_2$ | defined by equation (4) |
| $h_{1\mathrm{J}}$, $h_{2\mathrm{J}}$ | values of $h_1$, $h_2$ at a point on the junction AFE, figure 2 |
| $L$ | side of square plate |
| $L_0$ | defined by equation (1) |
| $m_0$ | yield moment |
| $m_1$, $m_2$ | principal moments |
| $m_u$, $m_v$ | principal moments in a hyperbolic field |
| $m_\alpha$, $m_\beta$ | principal moments in a parabolic field |
| $m_r$, $m_\theta$ | principal moments in a radial field |
| $n$ | number of sides of regular polygonal plate |
| $p$ | uniform pressure loading |
| $p_\mathrm{c}$ | collapse pressure |
| $q_u$, $q_v$ | shear forces in a hyperbolic field |
| $q_\alpha$, $q_\beta$ | shear forces in a parabolic field |
| $q_r$, $q_\theta$ | shear forces in a radial field |
| $r$ | radial polar coordinate |
| $R$ | length IQ, figure 4 |
| $R_0$ | length IP, figure 4 |
| $R_\mathrm{J}$ | length IJ, figure 4 |
| $s_1$, $s_2$ | distances along trajectories in a hyperbolic field |
| $s_{1\mathrm{J}}$ | value of $s_1$ at a point on the junction AFE, figure 2 |
| $u$, $v$ | orthogonal curvilinear coordinates in a hyperbolic field |
| $u_\mathrm{E}$ | value of $u$ at E, figure 2 |
| $u_\mathrm{J}(v)$ | value of $u$ at a point on the junction AFE, figure 2 |
| $v_\mathrm{E}$ | value of $v$ on DE, figure 2 |
| $v_\mathrm{J}(u)$ | value of $v$ at a point on the junction AFE, figure 2 |


PHILOSOPHICAL TRANSACTIONS OF THE ROYAL SOCIETY A MATHEMATICAL, PHYSICAL & ENGINEERING SCIENCES

| | |
|---|---|
| $w$ | small deflexion of the plate |
| $x, y$ | rectangular coordinates |
| $\alpha, \beta$ | orthogonal curvilinear coordinates in a parabolic field |
| $\gamma, \gamma_1$ | defined in figure 5 |
| $\Delta u, \Delta v$ | increments in $u$, $v$ for numerical calculations |
| $\zeta_u, \zeta_v$ | defined by equation (67) |
| $\eta = \partial w/h_2 \partial v$ | |
| $\theta$ | angular polar coordinate |
| $\kappa_1, \kappa_2$ | principal curvatures |
| $\kappa_u, \kappa_v$ | principal curvatures in anticlastic surface of mechanism |
| $\kappa_{uv} = 0$ | twisting curvature in anticlastic surface of mechanism |
| $\kappa_\alpha, \kappa_\beta$ | principal curvatures in developable surface of mechanism |
| $\kappa_s, \kappa_n, \kappa_{ns}$ | curvature components of mechanism for sections along and perpendicular to the junction AFE, figure 2 |
| $\lambda$ | hyperbolic net angle, figure 3 |
| $\lambda_\mathrm{J}$ | value of $\lambda$ at a point on the junction AFE, figure 2 |
| $\mu_1, \mu_2$ | defined by equation (64) |
| $\xi = \partial w/h_1 \partial u$ | |
| $\rho_1, \rho_2$ | radii of curvature of hyperbolic trajectories, equation (5) |
| $\rho_{1\mathrm{J}}, \rho_{2\mathrm{J}}$ | values of $\rho_1, \rho_2$ at a point on the junction AFE, figure 2 |
| $\chi(g)$ | defined by equation (53) |
| $\psi = \frac{1}{4}\pi - \lambda_\mathrm{J}$ | |

## 1. Introduction

In an earlier paper (Fox 1972) on limit analysis for rigid–perfectly plastic plates, the author gave the exact solution for the problem of a central point load on a simply supported rectangular plate of isotropic homogeneous material with yield in bending governed by the square yield criterion. The solution exemplified the possible complexity of exact solutions in this field, even when the loading and edge conditions are apparently simple. In the present paper, the exact solution is given for the problem of a uniformly distributed load on a clamped square plate of isotropic homogeneous material obeying the square yield criterion in bending. This exact solution is also complex with a mechanism consisting of a combination of developable and anticlastic surfaces, together with undeflected corner regions. The analysis is extended to cover the case of a clamped plate of any regular polygonal shape under uniform pressure and results for the collapse load are compared with some known upper bounds.

## 2. Statement of main problem

We consider a square plate of side $L$ and uniform thickness subjected to a uniform lateral pressure $p$. For convenience of nomenclature we regard the plane of the plate as horizontal, with load and deflexion positive downwards and with moments and curvatures taken positive when sagging. The material of the plate is homogeneous and isotropic, and yield in bending is governed by the square yield criterion with a yield moment $m_0$ per unit length of plate in both sagging and hogging curvatures.

For analysis we shall work non-dimensionally by introducing the length $L_0$ defined by

$$L_0^2 = 4m_0/p, \tag{1}$$





PHILOSOPHICAL TRANSACTIONS OF THE ROYAL SOCIETY A MATHEMATICAL, PHYSICAL & ENGINEERING SCIENCES

so that in the subsequent notation all lengths in the plane of the plate represent multiples of $L_0$ while component moments per unit length represent multiples of $m_0$ and component shear forces per unit length represent multiples of $m_0/L_0$.

The conditions for an exact solution of a problem of limit analysis for rigid–perfectly plastic plates loaded in bending have been discussed in detail by the author elsewhere (Fox 1968). Here we summarize these conditions for the present problem. First we define a *statically admissible stress field* as one in which the moments and associated shear forces satisfy (*a*) equilibrium with uniform pressure over the plate area, and (*b*) the square yield criterion illustrated in figure 1 in terms of principal moments $m_1$, $m_2$ per unit length of plate. Thus any deformation occurs only for states on the perimeter of the square ABCD and states outside the square are prohibited. Secondly, we define a *mechanism* as a small virtual deflexion of the plate such that (*a*) the deflexion is continuous and the slopes are at least piecewise continuous over the plate area, and (*b*) the deflexion is zero at the edges of the plate.

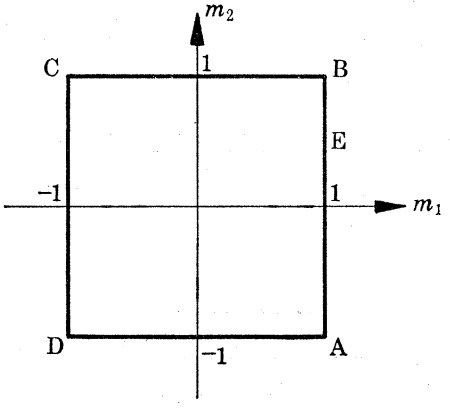


FIGURE 1. Square yield criterion.

For an exact solution, we must find a value $p_c$ of the pressure, called the *collapse pressure*, such that there coexist a statically admissible stress field and a mechanism related at all yielding parts of the plate by the *normality rule* defined below. The mechanism may contain variously (i) *rigid leaves* where the plate remains plane and undeformed, though a leaf may deflect as a rigid body, (ii) yielding regions of finite curvature, and (iii) *hinge-lines* corresponding to either (*a*) a discontinuity of slope across a boundary between two regions of the mechanism, or (*b*) non-zero normal slope on a clamped edge.

At a point in a yielding region of finite curvature in the mechanism, the *normality rule* can be specified in terms of principal moments $(m_1, m_2)$ and associated principal curvatures $(\kappa_1, \kappa_2)$ by the two conditions that (*a*) the directions of the principal curvatures coincide with the principal moment directions, and (*b*) a vector in the $(m_1, m_2)$ plane with components proportional to $(\kappa_1, \kappa_2)$ is in the direction of the outward normal to the yield locus ABCD (figure 1) at the associated point $(m_1, m_2)$ on ABCD. Thus for $(m_1, m_2)$ at E on the side AB, the second condition requires that $\kappa_1 > 0$, $\kappa_2 = 0$, while at the corners, regarded as limits of quadrants of circles of small radius (Fox 1968), the second condition requires that $\kappa_1 \geqslant 0$, $\kappa_2 \leqslant 0$, $\kappa_1 - \kappa_2 > 0$ at A and that $\kappa_1 \geqslant 0$, $\kappa_2 \geqslant 0$, $\kappa_1 + \kappa_2 > 0$ at B. On a hinge-line, the normality rule requires that the normal moment is a yield moment of the same sign as the hinge rotation.

In the present solution, we shall be concerned only with yielding states where $m_1 = 1$, $-1 \leqslant m_2 \leqslant 1$ corresponding to the side AB of the square yield locus of figure 1. We shall use the term *parabolic* region to denote any yielding region where $m_1 = 1$, $-1 < m_2 < 1$ at all internal points of the region, and the term *hyperbolic* region to denote that $m_1 = 1$, $m_2 = -1$ everywhere in a region. The stress field will be described and analysed in terms of a *moment net* consisting of two families of orthogonal curves such that at any point in the plane of the undeformed plate, the tangents to these curves are in the principal moment directions. These curves will be referred to as the *principal moment trajectories* and by the normality rule, they correspond also to the lines of curvature of the mechanism.

The search for an exact solution in the present field, other than by purely numerical methods, normally commences with some preconceived pattern for the moment net and the associated mechanism; accordingly, we shall next describe the main features of the present exact solution and then justify this solution by later analysis.

## 3. General description of the exact solution

In view of symmetry, we need consider only a triangular region forming one octant of the square plate as shown in figure 2, where C is the centre of the plate, B is a corner and A is the centre of one edge. The broken curve AFE is the junction between parabolic and hyperbolic moment nets illustrated in figure 2 and described below.

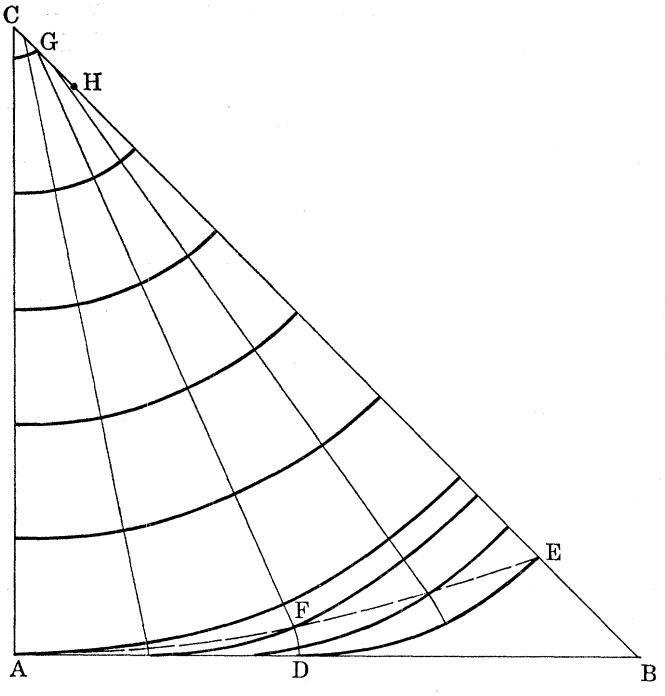


Figure 2. Moment net in the deforming region of an octant of the plate.

### *Region* ACEFA (*figure* 2)

This is a parabolic region with the moment net formed by (i) a family of straight principal moment trajectories e.g. CA, GF, HE, joining points on CH to points on AFE, and (ii) an orthogonal family of curved trajectories. The normal moment on any straight trajectory is

$m_1 = 1$ throughout the region, while the other principal moment satisfies $m_2 = 1$ on CH, $m_2 = -1$ on AFE and $-1 < m_2 < 1$ elsewhere in the region. There is unit normal moment with zero twisting moment and shear force along both CA and CE where the field is in equilibrium with similar fields in the adjacent octants of the plate. The associated part of the mechanism is a developable surface with generators along the straight trajectories and with sagging curvature circumferentially. The surface has zero slope normal to the extreme generators CA and HE where it joins similar surfaces in adjacent octants with continuous deflexion, slope and curvature across CA and HE. But the portion CH of the diagonal of the square is a sagging hinge-line with zero hinge-angle at H and increasing hinge-angle from H to C.

*Region* AFEDA (*figure* 2)

This is a hyperbolic region with $m_1 = 1$, $m_2 = -1$ everywhere and the two families of principal moment trajectories are curves of the type shown in figure 2. The trajectories with normal moment $m_2 = -1$ are all tangential to the part AD of the plate edge, with DE as one extreme trajectory and a vanishingly small trajectory as the other extreme at A, where the junction AFE is also tangential to the edge. The normal moment, twisting moment and shear force along AFE are continuous across this junction to give equilibrium with the parabolic field in the region ACEFA. Moreover, the principal moment directions are continuous across AFE so that the trajectories in the two regions join with continuous slope at this junction. The mechanism in AFEDA is an anticlastic surface in which the deflexion, slopes and curvatures are continuous across AFE with those in the adjacent developable surface. But there is a discontinuity in the circumferential sagging curvature across DF within the anticlastic surface, and an associated discontinuity in sagging curvature across GF in the developable surface. The deflexion is zero along AD and DE which are hogging hinge-lines. The hinge-line DE is tangential to the edge at D and meets the diagonal at right angles at E.

*Region* DEB (*figure* 2)

In this region the plate remains undeformed in its original plane and any one of an infinite number of statically admissible stress fields in this region will suffice to complete an exact solution.

*The collapse pressure*

In dimensional units, the collapse pressure $p_c$ is an unknown to be determined; the corresponding unknown in our non-dimensional units in relation to figure 2 is the half-length of the side, namely AB = AC = $g(0)$ of the later analysis, where

$$g(0) = L/2L_0. \tag{2}$$

As described later, the present solution gives $g(0) = 1.636521$ and from (1) and (2), the corresponding rounded value of the collapse pressure is

$$p_c = 42.851 m_0/L^2. \tag{3}$$

## 4. The moment net in the hyperbolic region AFEDA (figure 2)

Referring to figure 3, we use orthogonal curvilinear coordinates $(u, v)$ corresponding to the principal moment trajectories through a typical point Q. Thus QR is a trajectory $u$ = constant with principal normal moment $m_u = 1$ and downwards shear force $q_u$ per unit length on a

section with outward normal Q$u$, while PQ is a trajectory $v$ = constant with principal normal moment $m_v = -1$ and downwards shear force $q_v$ per unit length on a section with outward normal Q$v$. Specific definitions of $u$ and $v$ will be made later; first we introduce $h_1$, $h_2$, positive by definition, to denote the Lamé parameters such that an element of length is given by

$$\mathrm{d}s^2 = h_1^2\,\mathrm{d}u^2 + h_2^2\,\mathrm{d}v^2, \tag{4}$$

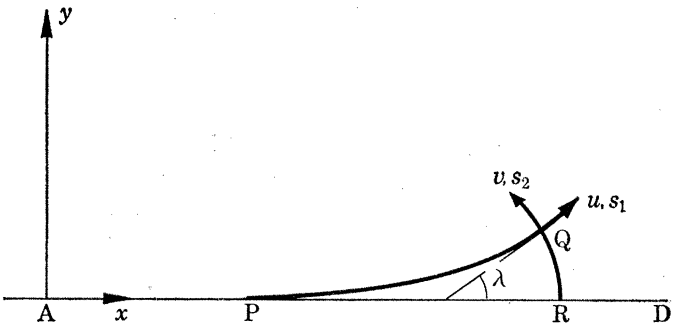


FIGURE 3. Notation for moment net in hyperbolic region.

and we use $s_1$, $s_2$, to denote distances along the trajectories. Also, we use $\lambda$ to denote the net angle (figure 3) defined as the anticlockwise rotation necessary to bring the positive $x$ direction into coincidence with the positive $u$ direction at the typical point Q (figure 3). We assume the following known relations for an orthogonal net which are easily derived:

$$\left.\begin{aligned} \frac{h_1}{\rho_1} &= \frac{\partial h_1}{h_2\,\partial v} = -\frac{\partial \lambda}{\partial u}, \quad \frac{\partial x}{h_1\,\partial u} = \cos\lambda = \frac{\partial y}{h_2\,\partial v}, \\ \frac{h_2}{\rho_2} &= \frac{\partial h_2}{h_1\,\partial u} = \frac{\partial \lambda}{\partial v}, \quad \frac{\partial y}{h_1\,\partial u} = \sin\lambda = -\frac{\partial x}{h_2\,\partial v}, \end{aligned}\right\} \tag{5}$$

where $\rho_1$, $\rho_2$ are the radii of curvature of trajectories $v$ = constant, $u$ = constant respectively, taken as positive if the trajectories are concave when viewed in the positive $v$ and $u$ directions respectively. Thus $\rho_1 < 0$, $\rho_2 > 0$ at Q in figure 3.

Hopkins (1957) has given the equations of equilibrium in curvilinear coordinates corresponding to the principal moment trajectories, and for the present case of uniform pressure and a hyperbolic field, these equations simplify to give in our notation and non-dimensional symbols:

$$\partial^2\lambda/\partial u\,\partial v + h_1 h_2 = 0, \tag{6}$$

$$\left.\begin{aligned} m_u &= 1, \quad m_v = -1, \\ q_u &= 2/\rho_2, \quad q_v = -2/\rho_1. \end{aligned}\right\} \tag{7}$$

Now on the trajectory QR (figure 3) where $\mathrm{d}u = 0$, and $h_2\,\mathrm{d}v = \mathrm{d}s_2$, it follows from (5) that $\partial\lambda/\partial u = -\mathrm{d}h_1/\mathrm{d}s_2$ and then from (6) we find that

$$\mathrm{d}^2h_1/\mathrm{d}s_2^2 - h_1 = 0 \quad (u = \text{constant}). \tag{8}$$

Similarly from (5) and (6) we find that

$$\mathrm{d}^2h_2/\mathrm{d}s_1^2 + h_2 = 0 \quad (v = \text{constant}). \tag{9}$$

Hence $h_1$, $h_2$ may be expressed in the forms

$$\left.\begin{aligned} h_1 &= f_1(u)\cosh s_2 - f_2(u)\sinh s_2, \\ h_2 &= f_3(v)\cos s_1 + f_4(v)\sin s_1, \end{aligned}\right\} \tag{10}$$

where

$$\partial s_1/\partial u = h_1, \quad \partial s_2/\partial v = h_2, \tag{11}$$

and $f_1, \ldots, f_4$ are at present arbitrary functions (the negative sign before $f_2$ in (10) is a convenience here as leading to a positive $f_2$ in our present problem). Equations (10) and (11) hold generally for any hyperbolic field under uniform pressure loading.

Referring to figure 3, we now specify $u$, $v$ by ($a$) the constant value of $u$ along RQ is $u = \mathrm{AR}$, and ($b$) the constant value of $v$ along PQ is $v = -\mathrm{AP}$. With these choices we have

$$u+v = 0 \quad \text{on the edge AD}, \tag{12}$$

$$u = 0, \quad v = 0 \quad \text{at A}, \tag{13}$$

and if we measure $s_1$, $s_2$ from the edge, then

$$s_1 = 0, \quad s_2 = 0 \quad \text{when} \quad u+v = 0. \tag{14}$$

We require PQ to be tangential to the edge AD since this is a hogging hinge-line, and if we temporarily let figure 3 refer to a point Q very close to P so that P is $(u, -u)$, R is $(u+\mathrm{d}u, -u-\mathrm{d}u)$ and Q is $(u+\mathrm{d}u, -u)$, then $\mathrm{PR} = \mathrm{d}u$, $\mathrm{QR} = h_2\,\mathrm{d}v = h_2\,\mathrm{d}u$, $\mathrm{PQ} = h_1\,\mathrm{d}u$ to the first order, and the tangential condition that $\mathrm{QR}/\mathrm{PQ} \to 0$, $\mathrm{PQ}/\mathrm{PR} \to 1$ as $\mathrm{d}u \to 0$, gives

$$h_1 = 1, \quad h_2 = 0 \quad \text{when} \quad u+v = 0. \tag{15}$$

Equation (15) would follow equally if the trajectories $v =$ constant (e.g. PQ) were tangential to a curved edge, and here we need the further condition that the edge AD is straight, namely

$$\lambda(u, -u) \equiv 0, \tag{16}$$

whence $\partial\lambda/\partial u = \partial\lambda/\partial v$ on the edge and then from (5) we find

$$\partial h_1/h_2\partial v + \partial h_2/h_1\partial u = 0 \quad \text{when} \quad u+v = 0. \tag{17}$$

The use of (11), (14), (15) and (17) in (10) leads to

$$\left.\begin{aligned} h_1 &= \cosh s_2 - f_2(u)\sinh s_2, \\ h_2 &= f_2(-v)\sin s_1, \end{aligned}\right\} \tag{18}$$

as the basic equations for the hyperbolic net in AFEDA (figure 2) where

$$s_1 = \int_{-v}^{u} h_1\,\mathrm{d}u, \quad s_2 = \int_{-u}^{v} h_2\,\mathrm{d}v, \tag{19}$$

in terms of integrals along trajectories $v =$ constant and $u =$ constant respectively.

We thus have one remaining arbitrary function $f_2(u)$ for use later when satisfying conditions on the junction AFE of figure 2. We denote this junction by $v = v_1(u)$, where $v_1(u)$ is at present unknown save that from (13) it must satisfy

$$v_1(0) = 0, \tag{20}$$

since the junction passes through A.

For a given positive $f_2(u)$, there is no intrinsic difficulty in the numerical evaluation of $h_1$, $h_2$, $s_1$ and $s_2$ from (18) and (19) by marching out from the edge, and in view of (5) and (18), the values of $\lambda$, $x$ and $y$ can then be evaluated, in particular, from

$$\left.\begin{aligned} \lambda &= \int_{-u}^{v} f_2(-v)\cos s_1\,\mathrm{d}v, \\ x &= u - \int_{-u}^{v} h_2 \sin\lambda\,\mathrm{d}v, \\ y &= \int_{-u}^{v} h_2\cos\lambda\,\mathrm{d}v, \end{aligned}\right\} \tag{21}$$

where the integrations are along the trajectory $u =$ constant through any typical point.

## 5. The moment net in the parabolic region ACEFA (figure 2)

In this region where the stress regime is $m_1 = 1$ and $-1 < m_2 < 1$ inside the region, the normality rule requires that $\kappa_2 = 0$ so that the mechanism is here a developable surface, while in the stress field one family of principal moment trajectories will be straight lines corresponding to the generators of the developable surface.

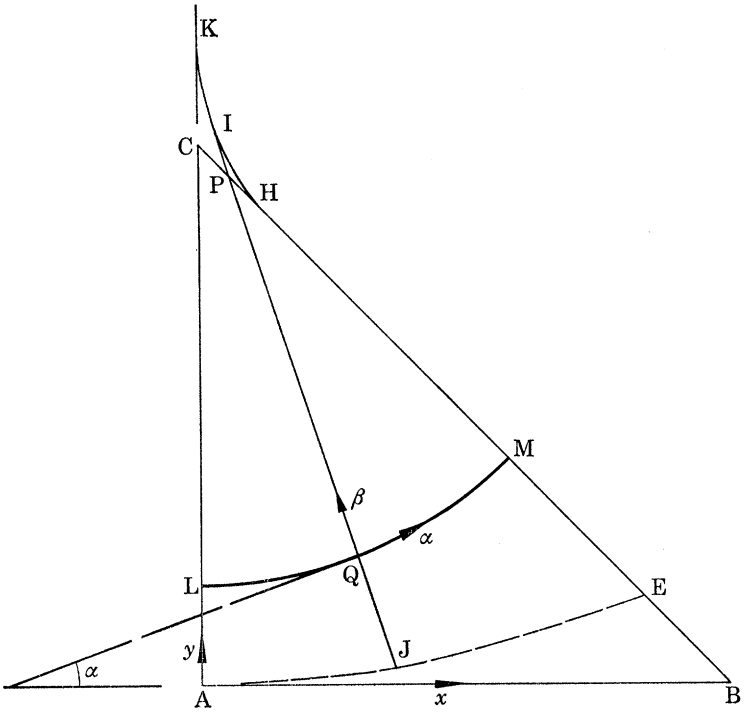


Figure 4. Notation for moment net in parabolic region.

Referring to figure 4, we use orthogonal curvilinear coordinates $(\alpha, \beta)$ analogous to $(u, v)$ of the previous section, so that $\alpha$ is constant on PQJ which is a typical straight trajectory meeting the junction in J and having normal moment $m_\alpha = 1$ and associated shear component $q_\alpha$, while $\beta$ is constant on the typical trajectory LQM with normal moment $m_\beta$ and shear component $q_\beta$. The family of straight trajectories will be tangential to some envelope such as HIK and the trajectory LQM will be an involute of HIK. We define $\alpha$ as equal to the net angle but we do not need to define $\beta$ specifically, since the equations of equilibrium for a parabolic field can be integrated generally (Collins 1971), with moments and shears expressed in terms of the net angle $\alpha$ and the radius of curvature IQ $= R$ (say) of LQM at any typical point Q. For uniform pressure, in the present non-dimensional notation, the field in the parabolic region is of the form

$$\left.\begin{aligned} m_\alpha &= 1, \\ m_\beta &= 1 - \tfrac{2}{3}R^2 + A(\alpha) + B(\alpha)/R, \\ q_\alpha &= 0, \\ q_\beta &= 2R - A(\alpha)/R, \end{aligned}\right\} \tag{22}$$

where $A(\alpha)$ and $B(\alpha)$ are arbitrary functions.

The extreme straight trajectories are CA and HE (figure 4) with principal normal moment $m_\alpha = 1$ and zero shear force, whence the field (22) will be in equilibrium across AC and HE with similar fields in the adjacent octants.

On CH, which is to be a sagging hinge-line in the mechanism, the normality rule requires that the normal moment on CH is the yield value of unity and since $m_\alpha = 1$, this requires that $m_\beta = 1$ also on CH; this then ensures that every direction through a point on CH is a principal direction with unit normal moment and zero twisting moment. Further, the normal moment will then be continuous across CH with the similar field in the adjacent octant. Secondly, for equilibrium with this adjacent field, we require zero shear force on CH which will be satisfied if $q_\beta = 0$ since this condition, with $q_\alpha = 0$ from (22), then ensures zero shear on a section in any direction through a point on CH. Thus if we write $R = R_0 = \mathrm{IP}$ on CH, we require

$$m_\beta = 1, \quad q_\beta = 0 \quad \text{when} \quad R = R_0, \tag{23}$$

which will be satisfied by (22) if we choose

$$A(\alpha) = 2R_0^2, \quad B(\alpha) = -\tfrac{4}{3}R_0^3, \tag{24}$$

in which $R_0$ will vary with $\alpha$. Thirdly, for a valid field in the region ACEJA (figure 4), it is necessary that the envelope KIH does not anywhere lie inside this region, and for this it is sufficient that

$$R_\mathrm{I} > R_0 \geqslant 0, \tag{25}$$

where $R_\mathrm{I} = \mathrm{IJ}$, and the equality sign will hold at H where CH touches the envelope KIH.

Noting that we shall later satisfy (25) and also $m_\beta = -1$ on the junction AJE (figure 4), it is easily verified from (22) and (24) that $m_\beta$ is monotonic decreasing from $m_\alpha = 1$ at P to $m_\beta = -1$ at J as $R$ increases on a typical trajectory PQJ, and the parabolic field is thus statically admissible.

## 6. Continuity conditions across the junction AFE (figure 2)

Referring to figure 5, SS is a portion of the junction curve AFE which is not a principal moment trajectory for either the parabolic field of coordinates $(\alpha, \beta)$ or the hyperbolic field of coordinates $(u, v)$, while NN is the normal to SS. Then without loss of generality, we may assume that

$$0 < \gamma_1 < \tfrac{1}{2}\pi, \quad 0 < |\gamma| < \tfrac{1}{2}\pi, \tag{26}$$

while the principal moments in the two fields will satisfy

$$\left.\begin{aligned} m_\alpha &= 1, \quad -1 \leqslant m_\beta \leqslant 1, \\ m_u &= 1, \quad m_v = -1. \end{aligned}\right\} \tag{27}$$

The continuity of normal moment across SS then gives

$$(1 - m_\beta)\cos^2\gamma_1 = 2\cos^2\gamma, \tag{28}$$

whence to satisfy the yield criterion $-1 \leqslant m_\beta \leqslant 1$, we need $\cos\gamma_1 \geqslant \cos\gamma$ so that (26) is replaced by

$$0 < \gamma_1 \leqslant |\gamma| < \tfrac{1}{2}\pi. \tag{29}$$

Secondly, in the associated parts of the mechanism we exclude the degenerate cases where either part is a plane and assume that the principal curvatures satisfy

$$\left.\begin{aligned} &\kappa_\alpha > 0, \quad \kappa_\beta = 0, \\ &\kappa_u \geqslant 0, \quad \kappa_v \leqslant 0, \quad \kappa_u - \kappa_v > 0. \end{aligned}\right\} \tag{30}$$

Now since SS is not in a principal moment direction, it cannot be a hinge-line and the adjacent surfaces of the mechanism must join with continuous slopes and have a common normal at any point on the junction. But then both the curvature component $\kappa_s$ along the junction and the twisting component $\kappa_{ns}$ must be continuous across the junction, whence we find

$$\left.\begin{aligned}\kappa_\alpha \cos^2\gamma_1 &= \kappa_u \cos^2\gamma + \kappa_v \sin^2\gamma,\\ \kappa_\alpha \sin 2\gamma_1 &= (\kappa_u - \kappa_v)\sin 2\gamma,\end{aligned}\right\} \tag{31}$$

and by eliminating $\kappa_u$ we obtain

$$\kappa_v \sin\gamma = \kappa_\alpha \cos\gamma_1 \sin(\gamma - \gamma_1). \tag{32}$$

Then from (29) and (30), the signs of the two sides in the second equation of (31) are only consistent if $\sin 2\gamma > 0$ whence $0 < \gamma < \frac{1}{2}\pi$, and the signs of the two sides in (32) are then only consistent if

$$0 < \gamma \leqslant \gamma_1 < \tfrac{1}{2}\pi. \tag{33}$$

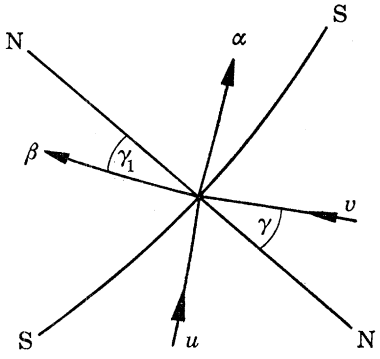


FIGURE 5. Notation at junction of parabolic and hyperbolic regions.

The condition (33), relating to the mechanism, is only consistent with (29), relating to the stress field, if

$$\gamma = \gamma_1 \tag{34}$$

so that the principal moment directions must be continuous across the junction. Then, from (28), (32) and (34) we must satisfy

$$m_\beta = -1 \tag{35}$$

in the parabolic field at the junction, and

$$\kappa_v = 0 \tag{36}$$

in the anticlastic mechanism at the junction.

We defer further consideration of the mechanism and concentrate on the stress field for which the remaining junction condition is continuity of shear which requires that

$$q_\beta = q_v + q_u \tan\gamma \tag{37}$$

on the junction.

We thus have the three conditions (34), (35) and (37) to be satisfied by the stress fields at the junction and we now consider these in detail. We shall regard the coordinate $u$ of the hyperbolic field as the basic independent variable along AFE (figure 2) with $v = v_j(u)$, at present unknown, along this junction. We use generally a suffix j, additional to any other suffixes, to denote values of field properties on the junction, and referring to figure 4 we shall write

$$\left.\begin{aligned}\mathrm{IP} &= R_0(u),\\ \mathrm{IJ} &= R_j(u),\\ \mathrm{PJ} &= g(u) = R_j(u) - R_0(u).\end{aligned}\right\} \tag{38}$$

Now the junction condition (34) means that the parabolic net is related geometrically to the hyperbolic net at the junction by the condition that any straight trajectory PJ (figure 4) is the tangent to the hyperbolic trajectory $u$ = constant through J. Thus referring to figure 6, the point I is the intersection of two such tangents at neighbouring points J, J′ on the junction where $\mathrm{JZ} = -h_{2\mathrm{J}}\,\mathrm{d}v$, $\mathrm{ZJ}' = h_{1\mathrm{J}}\,\mathrm{d}u$, $\mathrm{IP} = R_0$, $\mathrm{IJ} = R_\mathrm{J}$, $\mathrm{PJ} = g$, $\mathrm{P}'\mathrm{J}' = g + \mathrm{d}g$ and angle $\mathrm{PIP}' = \mathrm{d}\lambda_\mathrm{J}$ to the first order. It is then easily seen that $R_\mathrm{J}(u)$ is related to the hyperbolic field by

$$R_\mathrm{J}\frac{\mathrm{d}\lambda_\mathrm{J}}{\mathrm{d}u} = h_{1\mathrm{J}}, \tag{39}$$

while the condition that the point P, where $\mathrm{PJ} = g(u)$, lies on the diagonal requires that

$$\frac{\mathrm{d}g}{\mathrm{d}u} = -h_{2\mathrm{J}}\frac{\mathrm{d}v_\mathrm{J}}{\mathrm{d}u} - \frac{R_0}{R_\mathrm{J}}h_{1\mathrm{J}}\cot\left(\tfrac{1}{4}\pi - \lambda_\mathrm{J}\right). \tag{40}$$

The second junction condition (35), where $m_\beta$ is given by (22) and (24) with $R = R_\mathrm{J}$ and $R_0 = R_\mathrm{J} - g$, is satisfied if $R_\mathrm{J}$, $R_0$ and $g$ are related by

$$R_\mathrm{J} = \frac{2g^3}{3(g^2-1)}, \quad R_0 = \frac{g(3-g^2)}{3(g^2-1)}, \tag{41}$$

whence the condition (25) for the parabolic net requires that $g$ lies in the range

$$1 \leqslant g \leqslant \sqrt{3}, \tag{42}$$

and satisfies the end condition $\quad g = \sqrt{3} \quad \text{when} \quad \lambda_\mathrm{J} = \tfrac{1}{4}\pi$ (43)

at H (figure 4), where EH touches the envelope KIH with $R_0 = 0$.

Thirdly, the shear continuity condition (37) can, by using (7), (22), (24) and (41), be expressed as

$$-\frac{1}{\rho_{1\mathrm{J}}} + \frac{\tan\gamma}{\rho_{2\mathrm{J}}} = \frac{3+g^2}{2g}, \tag{44}$$

where from figure 6, $\quad \tan\gamma = -\dfrac{h_{2\mathrm{J}}}{h_{1\mathrm{J}}}\dfrac{\mathrm{d}v_\mathrm{J}}{\mathrm{d}u}.$ (45)

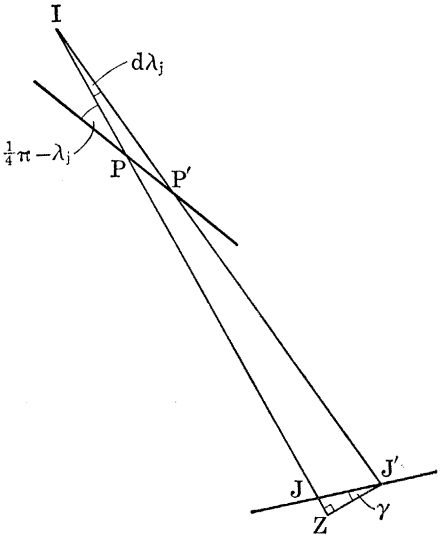


FIGURE 6

Then, by using (41) in (39) and (40) and by using (45) in (44), we can eliminate $R_j$, $R_0$ and $\gamma$ to obtain the three equations

$$\frac{d\lambda_j}{du} = \frac{3(g^2-1)}{2g^3} h_{1j}, \tag{46}$$

$$\frac{dg}{du} = -h_{2j}\frac{dv_j}{du} - h_{1j}\frac{3-g^2}{2g^2}\cot(\tfrac{1}{4}\pi - \lambda_j), \tag{47}$$

$$\frac{1}{\rho_{1j}} + \frac{h_{2j}}{h_{1j}\rho_{2j}}\frac{dv_j}{du} = -\frac{3+g^2}{2g}. \tag{48}$$

We now note that the hyperbolic net given by (18), (19) and (21) is completely determined if $f_2(u)$ is known and the junction is then determined if $v_j(u)$ is known. Thus the junction values $\lambda_j$, $h_{1j}$, $h_{2j}$, $\rho_{1j}$ and $\rho_{2j}$ in (46)–(48) can be regarded as functions of $f_2$ and $v_j$, and we have three equations (46), (47) and (48) corresponding to three basic unknowns $f_2(u)$, $v_j(u)$ and $g(u)$.

## 7. Evaluation of the stress field and the collapse load

Equations (46)–(48) can be recast in simpler form by noting first that, since

$$d\lambda_j/du = \partial\lambda/\partial u + (\partial\lambda/\partial v)\, dv_j/du$$

on the junction, it follows from (5) and (46) that

$$\frac{1}{\rho_{1j}} - \frac{h_{2j}}{h_{1j}\rho_{2j}}\frac{dv_j}{du} = \frac{-3(g^2-1)}{2g^3}, \tag{49}$$

and then equations (48) and (49) can be used to obtain separate expressions for $1/\rho_{1j}$ and $dv_j/du$. We can then use (5) and (18) to express $1/\rho_{1j}$ and $1/\rho_{2j}$ in terms of $f_2(u)$, $s_{1j}$ and $s_{2j}$ to give finally

$$\frac{dv_j}{du} = \frac{-h_{1j}}{f_2(-v_j)\cos s_{1j}}\left(\frac{3+g^4}{4g^3}\right), \tag{50}$$

$$\frac{dg}{du} = h_{1j}\left(\frac{3+g^4}{4g^3}\right)\tan s_{1j} - h_{1j}\left(\frac{3-g^2}{2g^2}\right)\cot(\tfrac{1}{4}\pi - \lambda_j), \tag{51}$$

$$f_2(u) = \frac{\tanh s_{2j} + \chi(g)}{1 + \chi(g)\tanh s_{2j}}, \tag{52}$$

where

$$\chi(g) = \tfrac{1}{4}g + \frac{3}{2g} - \frac{3}{4g^3}. \tag{53}$$

Equations (50)–(53) together with the end conditions (20) and (43) and the net equations (18), (19) and (21) give a determinate problem for finding the hyperbolic net in AFEDA (figure 2) and also $g(0)$, whence the collapse load follows as quoted earlier in (3).

The main strategic difficulty in the numerical evaluation of the solution over a fine mesh is that the net (18) is only easily computed by starting from A (figure 2), whereas the boundary condition (43) for $g(u)$ relates to the other end E of the net. This difficulty was overcome by starting with trial values of $g(0)$ to obtain a close estimate of most of the net, and then by using an iteration strategy. Details of the numerical method used for the present solution are outlined in the appendix A and here we state only the main features. For given $g(0)$, the net calculations marched out from $u = 0$, $v = 0$ at A with $u$ increasing in equal steps $\Delta u$, while for each $u$, the calculations marched out from $v = -u$ on the edge AB in equal steps $\Delta v = \Delta u$ in increasing $v$.

The calculations were carried out on the Cambridge University computer Titan with its normal precision of about eleven decimal digits. A finest mesh size of $\Delta u = \Delta v = 0.005$ was used, and also coarser mesh sizes of 0.01 and 0.02 in order to estimate the errors due to finite mesh size.

The most significant feature of the calculations with trial $g(0)$ is the behaviour of $g(u)$ which is illustrated in figure 7 by the divergence of the broken curves from the full curve given by the final solution following an iteration process described later. This divergence results from the dominance of the last term in (51) when the end condition (43) that $g \to \sqrt{3}$ as $\lambda_j \to \frac{1}{4}\pi$ is not satisfied exactly. Thus if the trial $g(0)$ is too large, then $g > \sqrt{3}$ with $dg/du > 0$ before $\lambda_j = \frac{1}{4}\pi$ and $g \to \infty$ as $\lambda_j \to \frac{1}{4}\pi$ with increasing $u$. On the other hand, if the trial $g(0)$ is slightly too small, then $g < \sqrt{3}$ with $dg/du < 0$ just before $\lambda_j$ reaches $\frac{1}{4}\pi$ and an accelerated decrease in $g(u)$ takes place down to $g = 1$ when from (46), $\lambda_j$ reaches a maximum and the desired condition $\lambda_j = \frac{1}{4}\pi$ at E (figure 2) is not attained.

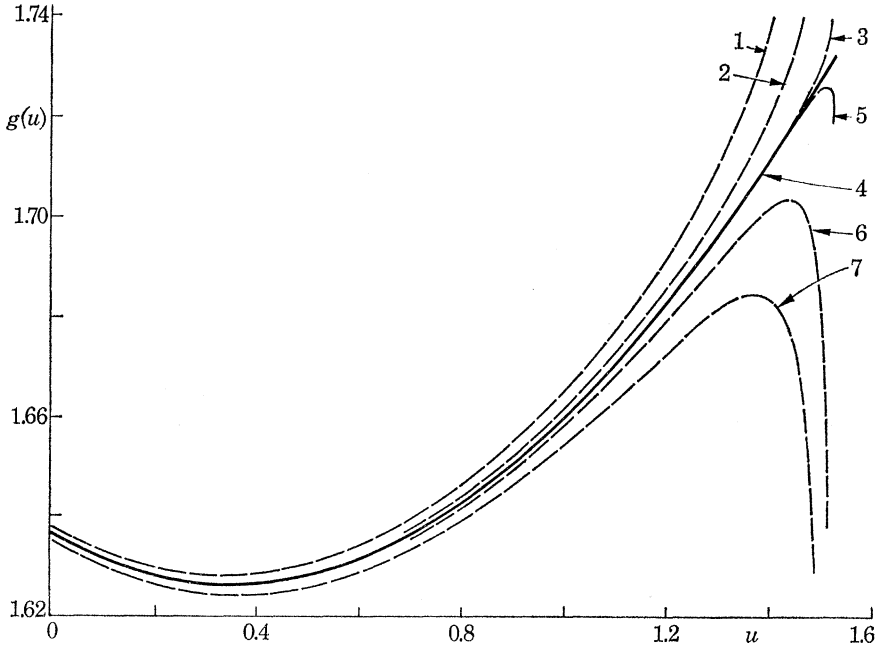


FIGURE 7. Variation of $g(u)$ with $u$ for $g(0) = 1.638$ (curve 1); 1.637 (curve 2); 1.63655 (curve 3); 1.636521 (curve 4); 1.6365 (curve 5); 1.636 (curve 6); 1.635 (curve 7).

It will be seen from figure 7 that a significant divergence of $g(u)$ from the stable exact solution takes place later as $g(0)$ approaches the exact $g(0)$ from above or below. But with a finite step size $\Delta u$ involving a finite step in $\lambda_j$, the final part of the net extending about one step from E cannot be reliably evaluated on this method. However, the results for trial $g(0)$ gave the very close bracket of 1.636514 to 1.636530 for the exact $g(0)$ with reliable calculations up to $u = 1.525$ for the finest mesh size $\Delta u = 0.005$.

We now note that $dg/d\lambda_j$ can be found from (46) and (51) and then the end condition (43) can be used to obtain the integral equation

$$2g(3-g^2)\sin\psi = \int_0^{\psi} (3+g^4)\,(\tan s_{1j})\sin\psi\,d\psi, \tag{54}$$

where

$$\psi = \tfrac{1}{4}\pi - \lambda_j, \tag{55}$$

so that $\psi$ decreases along the junction from $\frac{1}{4}\pi$ at A to zero at E.

Starting with $g = \sqrt{3}$ at $\psi = 0$, equation (54) enables $g(u)$ to be found numerically as a function of $u$ if $\psi$ and $s_{1\mathrm{J}}$ are known functions of $u$. Now the results for trial $g(0)$ close to the exact $g(0)$ did not exhibit any significant instability in junction properties other than $g(u)$ over the range of calculations. In particular, for both the close upper bound $g(0) = 1.636530$ and the close lower bound $g(0) = 1.636514$, the values of $\lambda_{\mathrm{J}}$ and $s_{1\mathrm{J}}$ remained stable with small third differences as $u$ increased for $u = 0(0.005)1.525$. Further, the changes in $\lambda_{\mathrm{J}}$ and $s_{1\mathrm{J}}$ with $g(0)$ for given $u$ were less than one-fifth of the change 0.000016 in $g(0)$ over the whole calculated range of $u$; in contrast, for $u = 1.525$, the change in $g(u)$ was about 500 times the change in $g(0)$. These results indicated that the calculated values of $\lambda_{\mathrm{J}}$ and $s_{1\mathrm{J}}$ for any $g(0)$ in the bracket 1.636514–1.636530 would be close estimates of $\lambda_{\mathrm{J}}$ and $s_{1\mathrm{J}}$ for the exact solution over the range $u = 0(0.005)1.525$. Also, since the exact solution will be stable up to $\lambda_{\mathrm{J}} = \frac{1}{4}\pi$, $\psi = 0$, close estimates of $u$ and $s_{1\mathrm{J}}$ for $\psi = 0$ can reasonably be obtained by extrapolation which involves only about one further step 0.005 in $u$.

The preceding observations led to the following method for the final evaluation of the exact solution. First, the mean value of the above bracket, namely $g(0) = 1.636522$, was used as a trial $g(0)$ to evaluate the net and junction properties for $u = 0(0.005)1.525$ and extrapolation was then used to find (i) the values of $\psi$ and $s_{1\mathrm{J}}$ at $u = 1.53$, (ii) the value $u = u_{\mathrm{E}}$ (about 1.53016) for $\psi = 0$, and (iii) the value of $s_{1\mathrm{J}}$ at $u = u_{\mathrm{E}}$. The values thus found for $s_{1\mathrm{J}}$ and $\psi$ were then used in a numerical evaluation of equation (54) to obtain values of $g$ for $u = 1.53(-0.005)0$, starting from $g = \sqrt{3}$ when $\psi = 0$ at $u = u_{\mathrm{E}}$. A succession of forward ($u$ increasing) and backward ($u$ decreasing) evaluations were then made in which ($a$) the values of $g(u)$ obtained in a backward run from (54) were used as input in a forward run with the earlier equations, excluding (51), to obtain revised values of $\psi$ and $s_{1\mathrm{J}}$ for $u = 0(0.005)1.53$, followed by extrapolation to obtain revised values of $u$ and $s_{1\mathrm{J}}$ for $\psi = 0$, ($b$) the revised values of $\psi$ and $s_{1\mathrm{J}}$ were used in a backward run of (54) to obtain revised values of $g(u)$. This process was stable with rapid convergence giving no changes within the accuracy of the calculations after the second backward run. This procedure was also carried out for step sizes $\Delta u = 0.01$ and 0.02 in order to estimate the effect of finite step size, and a comparison of the results indicated that the values of $g$, $\psi$ and $s_{1\mathrm{J}}$ were probably correct to $1 \times 10^{-8}$ for the smallest step size $\Delta u = 0.005$. In particular, all three step sizes agreed to seven significant figures in giving $g(0) = 1.636521$, leading to the result (3) given earlier for the collapse pressure.

For $\Delta u = 0.005$, the values of $g(u)$ obtained in the last run of the above iteration process were used in a final forward evaluation of all the main net and junction properties. Also, as an overall check on accuracy, the total load on the combined parabolic and hyperbolic region ACEDA (figure 2) was computed and compared with the calculated total shear reaction along ADE; these should be equal since there is no shear on AC and CE. The fractional error between the calculated values of total load and shear reaction was satisfactorily small at less than $1 \times 10^{-8}$.

Some features of the hyperbolic net are first that for given $u$ and increasing $v$, the values of $h_1$ decrease monotonically from unity on the edge to $h_{1\mathrm{J}}$ on the junction, while $h_2$, $s_1$, $s_2$ increase monotonically from zero at the edge to $h_{2\mathrm{J}}$, $s_{1\mathrm{J}}$, $s_{2\mathrm{J}}$ respectively on the junction. Secondly, in rounded values, as $u$ increases from zero at A to 1.530 at E, the values of $f_2(u)$ decrease smoothly from 1.155 at A to 1.081 at E, while junction properties vary smoothly and monotonically with $u$ as follows: (i) the distance along the junction from A increases from zero to 1.409 at E, (ii) $v_{\mathrm{J}}$ decreases from zero at A to $-0.753$ at E, (iii) $\lambda_{\mathrm{J}}$, $\gamma$, $h_{2\mathrm{J}}$, $s_{1\mathrm{J}}$, $s_{2\mathrm{J}}$ increase from zero at A to $\frac{1}{4}\pi$, 0.448, 0.723, 0.694, 0.305 respectively at E, and (iv) $h_{1\mathrm{J}}$ decreases from unity at A to 0.712 at E. Some further results for the net will be given later in comparison with upper bound solutions.



PHILOSOPHICAL TRANSACTIONS OF THE ROYAL SOCIETY A MATHEMATICAL, PHYSICAL & ENGINEERING SCIENCES

Having evaluated the properties of the hyperbolic net in AFEDA (figure 2) and of the junction, the calculation of the parabolic net in ACEFA is simple, based on the property that its straight trajectories are tangents on the junction to the trajectories $u$ = constant in the hyperbolic net.

To complete the stress field in the octant ABC (figure 2), we need to find any one statically admissible stress field in the corner region DEB, which remains plane and undeformed in the associated mechanism. The conditions to be satisfied by this field are: (i) equilibrium with uniform pressure, (ii) $-1 \leqslant m_1, m_2 \leqslant 1$, (iii) EB is a line of symmetry with zero shear and twisting moment, (iv) ED is a given principal moment trajectory with normal moment $m_2 = -1$ and (v) continuity of shear force across ED with the hyperbolic field in AFEDA (figure 2). There are no necessary boundary conditions for the stress field on the edge DB. All the preceding conditions will be satisfied if we can find a hyperbolic field of the type (10) in DEB, with net of the form illustrated in figure 8, where EB is the straight trajectory $u = 0$ while ED is the trajectory $v = 0$. For analysis of this field, we define the value of $u$, constant along a typical trajectory LM, by $u$ = arc length EM, while the value of $v$, constant along PN, is defined by $v$ = EN; also we measure $s_1$ from EB and $s_2$ from ED. With these choices,

$$\left.\begin{aligned} h_1 &= 1, \quad s_2 = 0 \quad \text{when} \quad v = 0, \\ h_2 &= 1, \quad s_1 = 0 \quad \text{when} \quad u = 0, \end{aligned}\right\} \tag{56}$$

and the given curvatures of EB and ED require that

$$1/\rho_2 = 0 \qquad \text{when} \quad u = 0, \tag{57}$$

$$1/\rho_1 = F(u) \quad \text{when} \quad v = 0, \tag{58}$$

where $F(u)$ is the variation of the curvature of ED with distance $s_1 = u$ along ED, and is known from the calculations for the adjacent hyperbolic net in AFEDA (figure 2). We note that since the positive directions of $u$ and $v$ convenient for the corner field (figure 8) are the reverse of those convenient in AFEDA (figure 3), the signs of $\rho_1, \rho_2$ are also reversed to conform with equation (5); in particular, $1/\rho_1 = F(u) > 0$ on DE for the corner field, while $1/\rho_1 = -F(u) < 0$ on DE for the field in AFEDA.

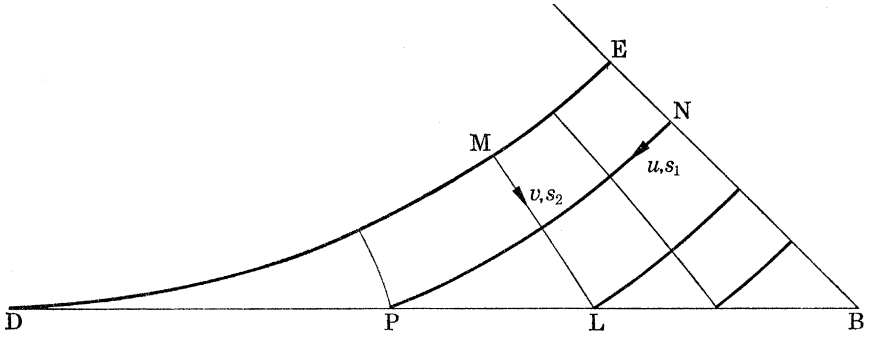


FIGURE 8. Moment net in the undeformed corner region DEB.

The use of (56)–(58) in the general form (10) leads to

$$\left.\begin{aligned} h_1 &= \cosh s_2 + F(u) \sinh s_2, \\ h_2 &= \cos s_1, \end{aligned}\right\} \tag{59}$$

which with use of (5) and (11) enables all properties of the net to be evaluated without difficulty by marching out from $u = 0$ on EB and $v = 0$ on ED. This field exists with $h_1 > 0$, $h_2 > 0$ over the whole region and is statically admissible.

We close this section by noting some general features of hyperbolic fields for uniform pressure loading. The basic equations are (10) and (11), and the field will exist provided $h_1 \geqslant 0$, $h_2 \geqslant 0$. Now on a hogging trajectory where $v$ is constant and $s_1$ is distance along the trajectory, it follows from (10) that $h_2$ must change sign when $s_1$ increases or decreases by $\pi$. Hence the field is limited in spatial extent in the $s_1$ direction by the condition that no hogging trajectory can have a length greater than $\pi$ in our non-dimensional units. At either boundary of the field in the $s_1$ direction, the hogging trajectories will be tangential to an envelope curve. This is illustrated in figure 2 where the edge AD is the special case of a straight envelope; it is of course possible to continue the field below AD by a similar 'mirror image' net, but there will then be a discontinuity of shear force along AD where both fields will exert a downward shear force of $-4/\rho_1$ on AD. In general, the bounding envelopes of a hyperbolic field for uniform pressure will only form part of a statically admissible field at a supported edge. The hyperbolic field for uniform pressure may also be limited in spatial extent in the $s_2$ direction by the condition $h_1 \geqslant 0$ depending on the signs and relative magnitudes of $f_1, f_2$ in (10). Thus for the corner net in DEB (figure 8), the given values of $F(u)$ as the curvature of DE suffice to define completely a net between a straight trajectory EB continued at either end, and a trajectory $u =$ constant through D. In fact, $F(u) > 1$ for the curve DE of our solution, whence from (59) the net could continue indefinitely with $s_2 > 0$ beyond the corner in the direction EB (though of limited width in the $s_1$ direction); but the net would necessarily cease when $h_1 = 0$ for sufficiently large negative $s_2$ in the reverse direction BE. On the other hand, for a different curve DE with a curvature satisfying $-1 < F(u) < 1$, a net of the form (59) could continue indefinitely in either direction along EB produced. In the present problem, apart from the given envelope AD for the net in AFEDA (figure 2), the hyperbolic nets in both AFEDA and DEB lie well inside the ranges of existence of the nets as governed by $h_1 \geqslant 0$, $h_2 \geqslant 0$. Nor is there any reason to expect that these conditions for existence of a hyperbolic field will lead to non-existence of exact solutions. Thus in our problem where a corner portion DEB and its mirror image in EB remain undeformed, the condition that arc DE $\leqslant \frac{1}{2}\pi$ for field existence simply means that we must expect the exact mechanism to extend at least near enough to the corner to satisfy this condition; in fact, it is very comfortably satisfied since arc DE $= 0.69$ in our solution.

A second general feature of hyperbolic nets for uniform pressure loading is that although the general form (10) contains four arbitrary functions, only two arbitrary functions remain after definite choices of $u$ and $v$. In general, given conditions along only two boundaries can be satisfied by the net in any particular problem. Thus the hyperbolic net in DEB (figure 8) is completely determined by the given sagging trajectory EB and the given hogging trajectory ED, while the hyperbolic net (18) in AFEDA (figure 2) contains only one arbitrary function after satisfying the one boundary condition that the given edge AD is an envelope of hogging trajectories.

## 8. Evaluation of the mechanism

As described earlier, the mechanism in an octant of the plate consists of a developable surface for the region ACEFA (figure 2) and an anticlastic surface for the region AFEDA, while the corner region DEB remains undeformed in its original plane. We commence with the consideration of the anticlastic surface where we regard the small deflexion $w$ as a function of the coordinates $(u, v)$ defined earlier for the associated hyperbolic stress field. We use the notation

$$\xi = \partial w/h_1 \partial u, \quad \eta = \partial w/h_2 \partial v, \tag{60}$$

for the component slopes of the mechanism and the component curvatures are then given by

$$\left.\begin{aligned} \kappa_u &= -\frac{\partial \xi}{h_1 \partial u} - \frac{\eta}{\rho_1}, \\ \kappa_v &= -\frac{\partial \eta}{h_2 \partial v} - \frac{\xi}{\rho_2}, \\ \kappa_{uv} &= -\frac{1}{h_1 h_2}\frac{\partial^2 w}{\partial u \partial v} + \frac{\xi}{\rho_1} + \frac{\eta}{\rho_2} \end{aligned}\right\} \tag{61}$$

on small deflexion theory with sagging curvatures positive.

Since the coordinates $(u, v)$ were defined as specifying the principal moment trajectories, it follows from the normality rule that these trajectories represent also the lines of curvature of the mechanism, with $\kappa_u$, $\kappa_v$ as principal curvatures. Thus the mechanism must satisfy $\kappa_{uv} = 0$, and from (61), (60) and (5), this condition can be expressed in either of the equivalent forms

$$\partial \eta / \partial u = \mu_1 \xi, \tag{62}$$

$$\partial \xi / \partial v = \mu_2 \eta, \tag{63}$$

where

$$\mu_1 = h_1/\rho_1, \quad \mu_2 = h_2/\rho_2. \tag{64}$$

All relevant properties of the net can be assumed known from the calculations for the stress field and we note in particular that

$$\mu_1 < 0, \quad \mu_2 > 0 \tag{65}$$

in AFEDA, and from (5) and (64) that

$$\partial \mu_1 / \partial v = -\partial^2 \lambda / \partial u \partial v = -\partial \mu_2 / \partial u. \tag{66}$$

The preceding equations with later boundary conditions enable the component slopes and the deflexion to be found numerically, but the subsequent evaluation of the curvatures from (61) would then involve the relatively inaccurate process of numerical differentiation. To avoid this, we introduce the notation

$$\zeta_u = h_1 \kappa_u, \quad \zeta_v = h_2 \kappa_v, \tag{67}$$

whence from (61) and (64) we find

$$\zeta_u = -\partial \xi / \partial u - \mu_1 \eta, \tag{68}$$

$$\zeta_v = -\partial \eta / \partial v - \mu_2 \xi, \tag{69}$$

and then from (68), (69), (62), (63), (64) and (66) it is easy to verify the relations

$$\partial \zeta_u / \partial v = \mu_1 \zeta_v, \tag{70}$$

$$\partial \zeta_v / \partial u = \mu_2 \zeta_u, \tag{71}$$

which can be used for a direct evaluation of $\zeta_u$, $\zeta_v$ and hence the curvatures.

The numerical evaluation of the anticlastic portion of the mechanism was carried out in two stages, commencing with the region DEF (figure 2). The basic boundary condition on the trajectory DE, where $v$ = constant = $v_E$ (say), is

$$w = 0 \quad \text{when} \quad v = v_E, \tag{72}$$

and then from (60) and (62) we find $\xi = 0$, $\eta$ = constant on DE. Now the deflexion $w$ is notionally very small, but since its overall magnitude is arbitrary and the governing equations are linear

in $w$, it is convenient for numerical evaluation to take $\eta = 1$ on DE. This is equivalent to expressing deflexions, slopes and curvatures as multiples of $\epsilon L_0$, $\epsilon$ and $\epsilon/L_0$ respectively, where $\epsilon$ is an arbitrary small positive number. The boundary conditions for the slopes are thus

$$\xi = 0, \quad \eta = 1 \quad \text{when} \quad v = v_{\mathrm{E}}, \tag{73}$$

and then from (68) we find

$$\zeta_u = -\mu_1 \quad \text{when} \quad v = v_{\mathrm{E}} \tag{74}$$

as a boundary condition for curvature. The other basic boundary condition in DEF is the junction condition (36) on EF, whence from (67),

$$\zeta_v = 0 \quad \text{when} \quad v = v_{\mathrm{J}}(u). \tag{75}$$

For known net properties, the differential equations (70) and (71) together with the boundary conditions (74) and (75) give a determinate problem for $\zeta_u$, $\zeta_v$ and there is no difficulty in finding these quantities numerically over a fine mesh in DEF by marching out from DE. The slopes and deflexion can be evaluated in the same programme by the numerical procedure outlined in appendix A. The calculations gave $\kappa_u > 0$, $\kappa_v \leqslant 0$ in agreement with the normality rule for the associated hyperbolic stress field. This agreement can be deduced without calculations as follows, direct from the governing equations. We consider the segment of any chosen trajectory $v =$ constant between DF and EF, noting that $u$ increases from DF to EF within DEF. Let $\zeta_{\mathrm{m}}(v)$ be the least value of $\zeta_u$ on this segment. Then if $\zeta_{\mathrm{m}} > 0$, we find (*a*) from (71), (65) and (75) that $\zeta_v \leqslant 0$ on the segment with the equality sign only on EF, (*b*) from (70) and (65) that $\partial\zeta_u/\partial v \geqslant 0$ at all points on the segment, whence $\mathrm{d}\zeta_{\mathrm{m}}/\mathrm{d}v \geqslant 0$. Thus if $\zeta_{\mathrm{m}}$ is positive on any segment, it is monotonic increasing with $v$, whence $\zeta_{\mathrm{m}} > 0$ and $\zeta_u > 0$, $\zeta_v \leqslant 0$ for all larger $v$ in DEF. But from (74) and (65), $\zeta_{\mathrm{m}} > 0$ on DE and it follows that $\zeta_u > 0$, $\zeta_v \leqslant 0$ everywhere in DEF, with $\zeta_u$ monotonic increasing with $v$ on a trajectory $u =$ constant, and $\zeta_v$ decreasing as $u$ decreases on a trajectory $v =$ constant. Lastly, we note that $h_1 > 0$, $h_2 \geqslant 0$, while from (5), (64) and (65), $\partial h_1/\partial v = h_2\mu_1 \leqslant 0$, $\partial h_2/\partial u = h_1\mu_2 > 0$ in DEF; hence from (67), $\kappa_u > 0$, $\kappa_v \leqslant 0$ in DEF with $\kappa_u$ increasing monotonically on a trajectory $u =$ constant as $v$ increases from DE to EF, while $\kappa_v$ decreases on a trajectory $v =$ constant as $u$ decreases from EF to DF.

We consider next the determination of the anticlastic surface in the region ADF (figure 2) and we note first the following properties of the net on the edge AD

$$h_1 = 1, \quad h_2 = 0, \quad \mu_2 = -\mu_1 = f_2(u) \quad \text{when} \quad u + v = 0, \tag{76}$$

which follow from earlier equations of § 4.

The basic boundary condition on AD is that

$$w(u, -u) \equiv 0, \tag{77}$$

with the resulting condition of zero slope along the edge, namely

$$\xi(u, -u) \equiv 0, \tag{78}$$

which after differentiation and use of (63), (76) and (68) leads to

$$\zeta_u(u, -u) \equiv 0 \tag{79}$$

as the boundary condition for curvature on the edge AD.





PHILOSOPHICAL TRANSACTIONS OF THE ROYAL SOCIETY A MATHEMATICAL, PHYSICAL & ENGINEERING SCIENCES

Also, on the edge AD where $v = -u$, we note for use in evaluating slopes, that

$$\mathrm{d}\eta/\mathrm{d}u = \partial\eta/\partial u - \partial\eta/\partial v = \zeta_v$$

by virtue of (62), (69) and (78), and since $\eta = 1$ at D by continuity, we find

$$\eta(u, -u) = 1 + \int_{-v_E}^{u} \zeta_v(u, -u)\,\mathrm{d}u. \tag{80}$$

The basic boundary condition on DF is that the deflexion is continuous across DF and equal to that found from the calculations for the mechanism in DEF. It follows, since all net properties are continuous, that the slope $\eta$ tangential to DF is continuous, and then since the condition $\xi = 0$ holds on both AD and DE from (78) and (73), it follows from (63) that $\xi$ is continuous across DF and from (69) that $\zeta_v$ is continuous across DF. Thus the boundary condition on DF for curvature is that

$$\zeta_v = \Phi(v) \quad \text{when} \quad u = -v_E, \tag{81}$$

where $\Phi(v)$ is a function known numerically from the calculations for the region DEF. Lastly, we again have the curvature boundary condition (75) on the junction AF.

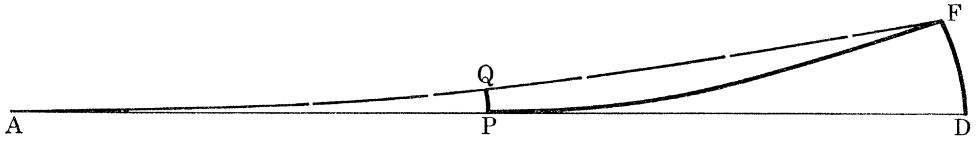


FIGURE 9

To determine $\zeta_u$, $\zeta_v$ in ADF, we have the three boundary conditions (75), (79) and (81) which at first sight appear too many for the two first order differential equations (70) and (71). However, the conditions (75) and (81) do not operate together in determining the values of $\zeta_u$, $\zeta_v$ at any given point in ADF. The differential equations (70) and (71) are of hyperbolic type with effects on a boundary propagating along the characteristics which are here the net trajectories $u$ = constant and $v$ = constant. Thus, referring to figure 9, equations (70) and (71) and the boundary conditions (79) and (81) suffice to determine the values of $\zeta_u$, $\zeta_v$ in the sub-region PFD and these values are unaffected by the boundary condition (75) on AF. Then for the sub-region PQF we again have only two boundary conditions, namely (75) on QF and given $\zeta_u$ on PF as determined by continuity of $\zeta_u$ with the field in PFD; this problem is of the same type as that for the earlier region DEF and has a unique solution giving, in particular, values of $\zeta_v$ on QP. Then for AQP, the problem is similar to the original problem for ADF, and hence there is a unique solution in ADF corresponding to a succession of sub-regions of the types PFD and PQF. However, although analytically the determination of the mechanism in ADF is most logically regarded in terms of an infinite sequence of sub-regions, there is no difficulty in obtaining a numerical solution in a direct manner by marching out from DF with $u$ decreasing in steps, where at each step the evaluation of mechanism properties is carried out for the full range of $v$ from the edge to the junction (see appendix A). The calculations gave $\kappa_u \geqslant 0$, $\kappa_v \leqslant 0$ in ADF in agreement with the normality rule for the associated hyperbolic stress field. Again, this result can be deduced direct from the governing equations and the boundary conditions in an analogous manner to that given earlier for DEF, save that (*a*) the argument is applied to the successive sub-regions of figure 9, and (*b*) the roles of $u$, $v$ and of $\zeta_u$, $\zeta_v$ are interchanged in the argument for a sub-region of the type PFD.

An interesting result of the calculations for the mechanism in the anticlastic region AFEDA (figure 2) is the very rapid decrease of $\zeta_u$ and $-\zeta_v$ as $u$ decreases from D to A in the region ADF. Thus $\zeta_u$ is a maximum on the junction for given $u$, and starting from about 0.2 at F, the junction values of $\zeta_u$ decrease to about 0.002 by $u = 0.377$ corresponding to Q in figure 9, and then to order $10^{-10}$ by $u = 0.1$ and to order $10^{-19}$ by $u = 0.025$. Similarly, the maximum values of $-\zeta_v$ occurring on the edge AD and starting from about 0.8 at D, decrease to about 0.03 by $u = 0.377$ and then to order $10^{-8}$ by $u = 0.1$ and to order $10^{-17}$ by $u = 0.025$ (note that $u$ is distance from A along AD). In agreement, it is shown in appendix B that $\zeta_u$, $\zeta_v$ are not analytic functions of $u$ at A, since they decay to zero faster than any finite power of $u$ as $u \to 0$ at A. Since $h_1$ is of order unity it follows that $\kappa_u$ is similarly very small near A. But $h_2 = 0$ on the edge AD where $\kappa_v$ is infinite except at A; however, the smallness of $\zeta_v$ implies that $\kappa_v$ will be very small near A except in a very narrow band near the edge. Moreover, from (68), (69) and (80), the slopes are related to the curvatures through $\zeta_u$, $\zeta_v$, and similarly for the energy dissipation over an element of area which is $(\kappa_u - \kappa_v) h_1 h_2 \mathrm{d}u \mathrm{d}v = (h_2 \zeta_u - h_1 \zeta_v) \mathrm{d}u \mathrm{d}v$. It follows that so far as slopes, deflexion and energy dissipation are concerned, the portion of the mechanism near A in ADF approximates very closely to a plane surface through the edge. This is also illustrated by the curve in figure 10 for the variation of the hinge angle along AD which becomes effectively constant to within 0.3 % for $u < 0.4$.

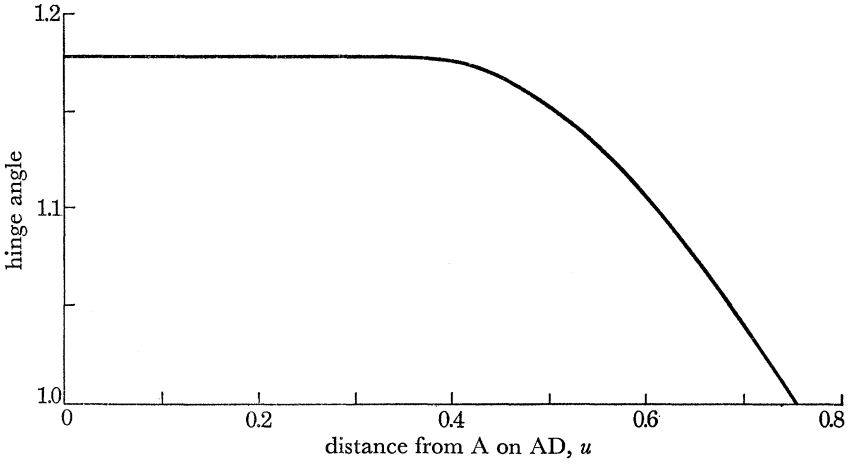


FIGURE 10. Variation of hinge angle along AD.

We note from (74) that $\zeta_u = -\mu_1$ on DE and is about 1.13 at D, while from (79), $\zeta_u = 0$ at D on AD, so there is a discontinuity in $\zeta_u$ across DF at D. Further, since $\mu_1 \zeta_v$ is continuous across DF it follows from (70) that there is a constant discontinuity of about 1.13 in $\zeta_u$ across DF; and since $\zeta_u = h_1 \kappa_u$, there will be an associated discontinuity in the circumferential curvature $\kappa_u$, but it will not be constant since $h_1$ varies along DF. The discontinuity is evident in figure 11, which gives the variation of $\kappa_u$ along the junction and along DE, noting that $\kappa_u = 0$ along AD, while for $u < 0.4$, the junction values of $\kappa_u$ are too small to show in the figure. Within the region AFEDA (figure 2), $\kappa_u$ increases monotonically with $v$ for given $u$, so that figure 11 gives the extreme values of $\kappa_u$ in the anticlastic surface.

The unique solution obtained for the anticlastic surface in AFEDA determines in particular the values of the deflexion $w$ and the slope $\eta$ on the junction. The mechanism in the parabolic region ACEFA (figure 2) can then be defined geometrically as the ruled surface formed by the

continuation in the $v$-direction of tangents to the anticlastic surface along the junction. This gives continuity of $w$ and the component slope $\eta$, and since the slope along the junction, at an angle to the $v$-direction, is continuous since $w$ is continuous, it follows that the other component slope $\xi$ is also continuous. Further, if $s$, $n$ denote directions along and normal to the junction, then the continuity of slopes gives continuity of the curvature components $\kappa_s$, $\kappa_{ns}$, while the curvature component $\kappa_v = 0$ in the anticlastic surface on the junction is continuous with the zero curvature component along a generator of the ruled surface. The continuity of $\kappa_s$, $\kappa_{ns}$ and $\kappa_v$, where $v$ is at an angle to $n$ and $s$, gives the same Mohr's circle for curvature in both surfaces, so that the principal directions of curvature and the principal curvatures are continuous across the junction. We can now use these continuity conditions, in conjunction with known properties of ruled surfaces (Weatherburn 1930), to verify that the normality rule is satisfied in the parabolic region ACEFA, where we shall again use the coordinates $(\alpha, \beta)$ of § 5.

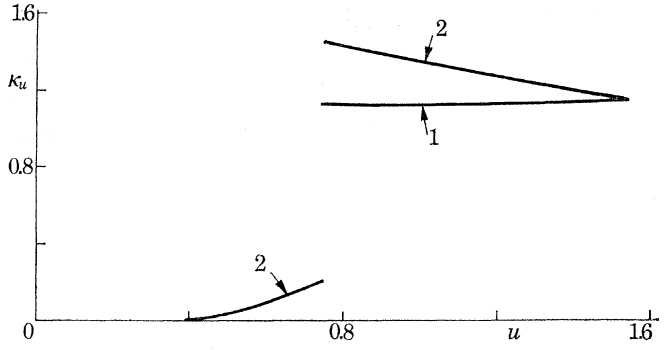


FIGURE 11. Circumferential sagging curvature on (1) DE, (2) junction AFE.

It is a known property of a ruled surface that along a given generator, the Gaussian curvature $\kappa_1\kappa_2$ is inversely proportional to the fourth power of a distance function which is here the length $R = \mathrm{IQ}$ of figure 4. But the Gaussian curvature of our ruled surface is zero on the junction since $\kappa_2$ is there continuous with the zero junction value of $\kappa_v$ in the anticlastic surface. It follows that the Gaussian curvature is zero everywhere in the ruled surface which is therefore developable with principal curvatures $\kappa_1 = \kappa_\alpha$, $\kappa_2 = \kappa_\beta = 0$. Secondly, from a known property of a developable surface, the product $R\kappa_\alpha$ is constant along a given generator, and since $\kappa_\alpha = \kappa_u \geqslant 0$ on the junction, it follows that $\kappa_\alpha \geqslant 0$ everywhere in the surface. Hence the mechanism in ACEFA has principal curvatures $\kappa_\alpha \geqslant 0$, $\kappa_\beta = 0$, which satisfy the normality rule in relation to the associated parabolic stress field of principal moments $m_\alpha = 1$, $-1 \leqslant m_\beta \leqslant 1$.

Since there is no twist along a generator of the developable surface, the component slopes of the surface along and normal to a given generator are constant along the generator and equal to the slopes $\eta_\mathrm{J}$, $\xi_\mathrm{J}$ respectively of the anticlastic surface on the junction. Now from (73) and (78) we note that $\xi_\mathrm{J} = 0$ at the ends E and A of the junction; it follows that the circumferential slope is zero along both the extreme generators AC and EH, where the surface will thus join similar surfaces in adjacent octants with continuous slopes. On CH, the adjacent parts of the mechanism join in a sagging hinge of angle which increases monotonically from zero at H to about 1.67 at C. The deflexion on CH is plotted in figure 12 where it is seen that it does not differ much from a linear variation with distance corresponding to the generator EH produced. As the circumferential curvature $\kappa_\alpha$ in the developable surface is the same on the junction as that given in figure 11 for the anticlastic surface, and since $R\kappa_\alpha$ is constant along a generator, it follows that

(*a*) $\kappa_\alpha$ is infinite at H where $R = 0$, (*b*) $\kappa_\alpha$ is discontinuous across GF, and (*c*) $\kappa_\alpha$ is very small near AC where the developable surface approximates closely to a plane.

The relative smallness of the curvature in the region ACGFDA (figure 2) is also indicated by the fact that this curvature contributes only about 2 % of the total energy dissipation in the mechanism. This compares with about (i) 46 % from the curvature in the region DFGED, (ii) 4 % from the sagging hinge CH, (iii) 27 % from the hogging hinge AD, and (iv) 21 % from the hogging hinge DE. It is also of interest to note that the curvature in the anticlastic region AFEDA contributes only about 4 % of the total energy dissipation in comparison with about 44 % from the curvature in the developable region ACEFA.

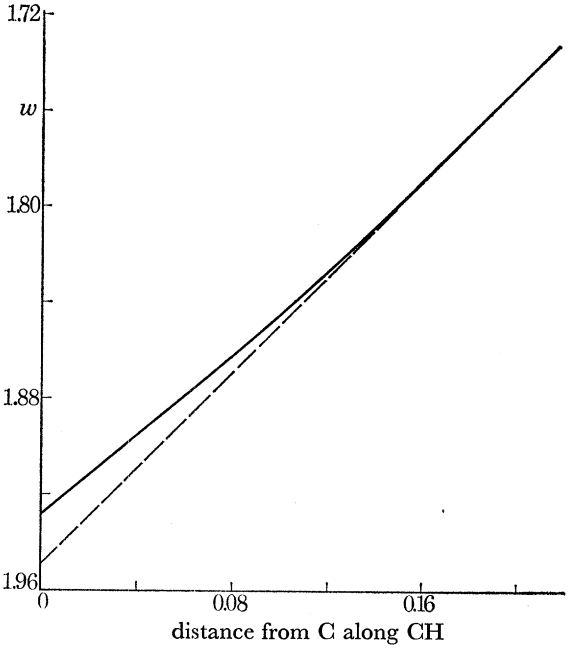


FIGURE 12. Deflexion on CH (full curve) compared to deflexion on generator EH produced (broken line).

## 9. COMPARISON OF THE EXACT SOLUTION AND SOME KNOWN UPPER BOUND SOLUTIONS

The exact solution will now be compared with three known upper bound solutions having mechanisms of regional pattern shown in figures 13 *a*, *b* and *c* for one octant of the plate. The lettering in these figures has been chosen as far as possible so that the different regions of the mechanisms are generally similar in type to those of the exact solution with the same lettering in figure 2. In all cases, C is the centre of the plate while B is a corner and AB is half of one side of the plate. We note that in all solutions, a corner portion DEB remains undeformed in its original plane and we describe below the shape of the deforming region for each mechanism.

Mansfield (1957) extended the scope of upper bound solutions for a variety of problems by using the calculus of variations. In particular, for the present problem he proposed the pattern of figure 13 *a*, where (i) the part ACD rotates as a rigid leaf about the edge AD, with C deflecting to C′ (say), and (ii) the portion DCE deforms as part of a general conical surface with base curve DE and vertex C′. The calculus of variations was used to find the shape of the curve DE giving the least collapse pressure for the pattern.

Wood (1961) employed the pattern of figure 13*b*, where DE is a circular arc of centre H and is tangential to the edge at D. The plate deformation is (i) the part ACHD remains plane and rotates as a rigid leaf about the edge AD, with H deflecting to H′ (say), and (ii) the part DHE deforms as part of a circular cone with base curve DE and vertex H′. The ratio CH/CB was chosen to give the smallest collapse pressure for this pattern of deformation.

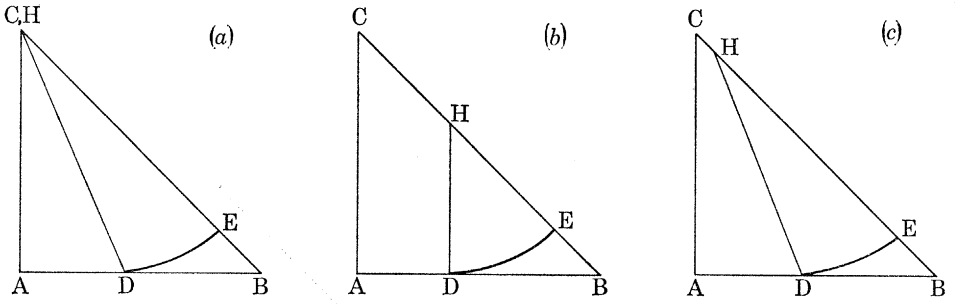


FIGURE 13. Regional patterns for upper bound solutions: (*a*) Mansfield; (*b*) Wood; (*c*) Mansfield–Morley.

TABLE 1. COMPARISON OF EXACT AND UPPER BOUND SOLUTIONS FOR A CLAMPED SQUARE PLATE UNDER UNIFORM PRESSURE

| | exact | Mansfield–Morley | Mansfield | Wood |
|---|---|---|---|---|
| $p_c L^2/m_0$ | 42.851 | 42.880 | 42.895 | 43.852 |
| AD/AB | 0.46001 | 0.44513 | 0.44161 | 0.39596 |
| CE/CB | 0.84225 | 0.84075 | 0.84061 | 0.82308 |
| CH/CB | 0.09386 | 0.06672 | 0 | 0.39596 |
| CG/CB | 0.03899 | — | — | — |

Morley (1965) extended Mansfield's solution by taking the vertex of the cone off-centre at H in plan in figure 13*c*; this introduced an extra parameter CH/CB for use with Mansfield's shape of DE and this ratio was chosen to give the smallest collapse load. Following Wood (1969), we shall refer to this mechanism as the Mansfield–Morley solution.

All three upper bound mechanisms are qualitatively similar in that they contain a rigid leaf, a conical surface and an undeformed corner region. The exact mechanism is more complex in that the deforming portion consists of a more general developable surface and an anticlastic surface. However, there is a general qualitative similarity between the exact mechanism and the upper bound mechanisms, noting that (i) the anticlastic region is relatively narrow, (ii) there is a discontinuity of circumferential curvature across GFD (figure 2) in the exact mechanism and across HD in the upper bound mechanisms, and (iii) the exact mechanism approximates closely to a plane near AC. In particular, there is a marked similarity between the exact mechanism and the Mansfield–Morley mechanism.

For the present comparison, numerical results for the upper bound mechanisms have been recalculated to the same accuracy as the exact solution and rounded results are given in table 1. This table lists the collapse pressure and some relevant dimensions of the regional patterns for both the exact (figure 2) and upper bound (figure 13) mechanisms. It is seen that the Mansfield and Mansfield–Morley solutions give very close estimates of the exact collapse pressure, within about 0.1 %, while Wood's simpler solution gives a value only about 2.3 % high.

As indicated by the ratios AD/AB and CE/CB in table 1, the exact mechanism extends nearer the corner than any of the upper bound mechanisms. Though this extension is very small in

relation to the Mansfield and Mansfield–Morley mechanisms for which the arcs DE lie close inside the exact arc DE along its whole length, within normal distances of 0.0026 AB and 0.0022 AB respectively.

## 10. The exact solution as the limiting case of sequences of upper and lower bound solutions

The theory of limit analysis for plates implies that an exact solution should correspond to the limiting case of at least one continuous sequence of upper bound mechanisms and at least one continuous sequence of statically admissible stress fields forming lower bound solutions. Such sequences can be defined for the present problem in terms of results for trial $g(0)$ discussed earlier in § 7. We note that for any given $g(0)$, the associated pressure is given from (1) and (2) by

$$pL^2/m_0 = 16[g(0)]^2 \tag{82}$$

and that the hyperbolic field and associated junction and parabolic field can be evaluated by marching out from A (figure 2) to obtain a stress field which is certainly statically admissible while $g(u)$ remains in the range $1 \leqslant g(u) \leqslant \sqrt{3}$ of equation (42).

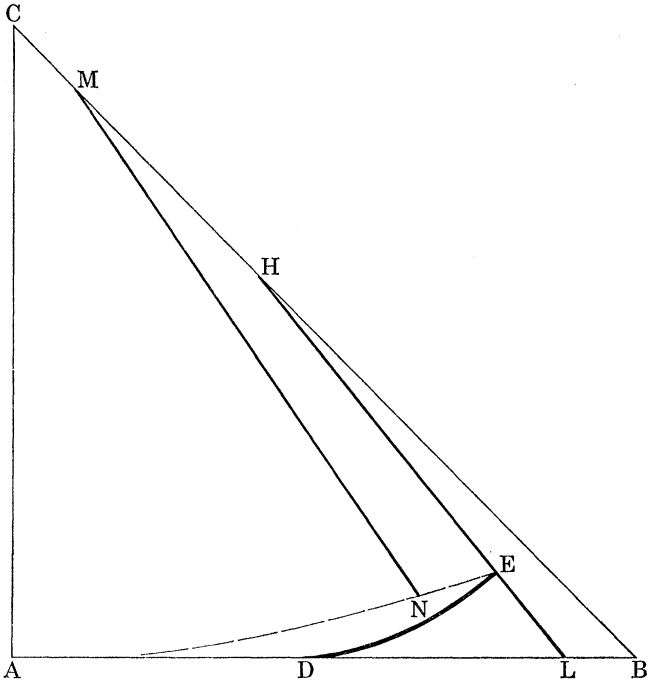


Figure 14. Regional pattern for lower bound solution.

Consider a trial $g(0)$, e.g. 1.635, for which the pressure $p$ of equation (82) is a close lower bound to the collapse pressure $p_c$ of equation (3). Then as $u$ increases in figure 7, we see that $g(u)$ at first decreases to a minimum value $> 1$ and then increases to a maximum value less than $\sqrt{3}$, followed by a rapid decrease which will continue at least to $g = 1$ at $u = u_1$ (say). Thus for $0 \leqslant u \leqslant u_1$ there is a statically admissible stress field corresponding to a moment net over a region ACHEDA of the type illustrated in figure 14, where HE = 1 and MN represents the maximum value of $g(u)$. For clarity, figure 14 is not to scale for a close lower bound since, if for example $g(0) = 1.635$, the

true angles NMB and EHB are less than 4°. Now the calculations and analysis indicate that for any lower bound $g(0)$ between 1.635 and the exact $g(0)$, the length HB is about $1.4 < \sqrt{3}$; hence to complete a statically admissible stress field in the octant, we consider first the sector LHB (figure 14) where, using polar coordinates $r$, $\theta$ with origin H, we specify the simple radial field of principal moments $m_r$, $m_\theta$ given in our non-dimensional units by

$$\left.\begin{aligned} m_\theta &= 1, \quad m_r = 1 - \tfrac{2}{3}r^2, \\ q_\theta &= 0, \quad q_r = -2r, \end{aligned}\right\} \tag{83}$$

which is statically admissible since $0 \leqslant r < \sqrt{3}$, and satisfies the necessary stress continuity conditions across HE. Secondly, in the region DEL (figure 14) we can, as for the exact solution, find a hyperbolic field of the type (59) having EL and DE as given principal moment trajectories. This completes a statically admissible stress field for the typical octant, noting that there is unit normal moment, zero twisting moment and zero shear force along both AC and CB to satisfy continuity conditions with similar fields in adjacent octants of the plate. Such a statically admissible stress field will exist at least for all pressures $p$ given by (82) when $g(0)$ lies between 1.635 and the exact $g(0)$. Hence if we consider $g(0)$ increasing continuously in this range, there will be a continuous sequence of lower bound solutions in which the angles NMB and LHB of figure 14 decrease steadily to zero to give the exact stress field as the limiting case for the exact $g(0)$ and $p = p_c$.

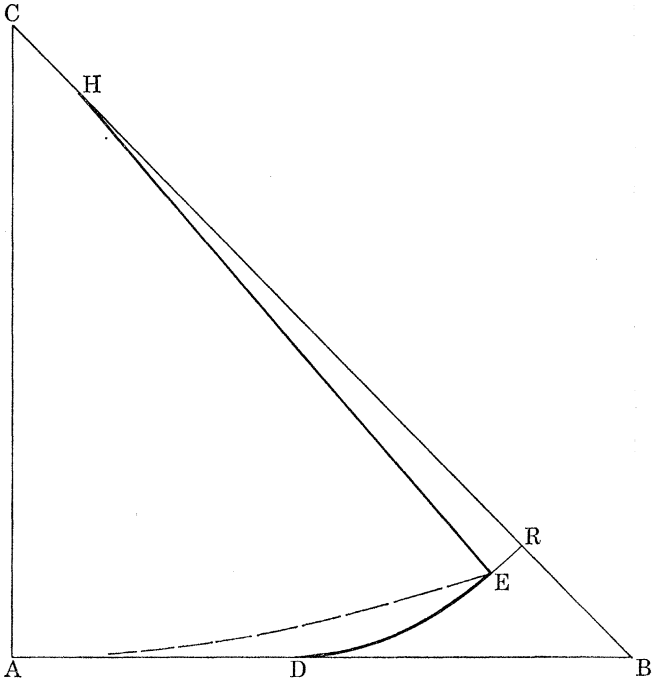


FIGURE 15. Regional pattern for upper bound solution.

Consider next a value of $g(0)$, e.g. 1.638, for which the pressure $p$ of equation (82) will be a close upper bound to the collapse pressure. For such $g(0)$ with increasing $u$ in figure 7, we see that $g(u)$ at first decreases to a minimum value $> 1$ and then increases steadily to reach the value $\sqrt{3}$ at $u = u_2$ (say). Then for $0 \leqslant u \leqslant u_2$, there is a statically admissible stress field corresponding to a moment net over a region of the type ACHEDA shown in figure 15, where HE $= \sqrt{3}$

while ER is a circular arc of centre H. We note that for any $g(0)$ between 1.638 and the exact $g(0)$, the angle EHB is less than 4°. Now the analysis of § 8 for the exact mechanism can be equally applied to find a surface of similar type which satisfies $w = 0$ on ADE and the normality rule in relation to the moment net in the region ACHEDA of figure 15. Then if H deflects to H′ in this surface, we add part of a circular cone of vertex H′ and base curve ER to complete the mechanism in the octant, with the corner portion DRB remaining undeformed in its original plane. There are similar surfaces in adjacent octants giving a sagging hinge on CH and continuity of deflexion and slope across AC and HR.

It remains to show that the application of the upper bound theorem to the above mechanism, derived for a given $g(0)$, leads to the value of $p$ given by (82). For this purpose, we shall first show that the mechanism is an exact mechanism for loading by the uniform pressure $p$ plus a line load along ER; and to do this we need the associated stress field. Now from the above definition of the mechanism in ACHEDA (figure 15), it will in this region satisfy the normality rule in association with the statically admissible stress field calculated for the trial $g(0)$. Then in EHR, the simple radial field (83) which gives $m_r = -1$ on ER where $r = \sqrt{3}$, will be statically admissible for the pressure $p$ and satisfy (i) the necessary stress continuity conditions across HE and (ii) the normality rule for the associated conical portion of the mechanism. Also, the combined stress field in ACRDA and similar fields in adjacent octants will satisfy the necessary stress continuity conditions across AC and CR. Lastly, in the corner region DRB we can use a hyperbolic field of the type (59) with given principal moment trajectories DR and RB; this field will be statically admissible for the pressure $p$ and satisfy all necessary continuity conditions across DR and RB except for a discontinuity of shear force along ER which can be balanced by an upward line load of intensity $2\sqrt{(\frac{1}{3}pm_0)}$ per unit length in dimensional units. We therefore obtain a mechanism and stress field giving the exact solution for loading by uniform pressure $p$ and the line load along ER. But this line load does no work on the mechanism; hence the application of the principle of virtual work using the mechanism and the equilibrium of the stress field with the loading, will give an equation for $p$ which is identical with that given by the upper bound theorem for this mechanism and loading by pressure $p$ only. Thus for uniform pressure loading, upper bound mechanisms of the above type with pressures $p$ given by (82), will exist at least for all $g(0)$ lying between 1.638 and the exact $g(0)$; hence if we consider $g(0)$ decreasing continuously in this range, there will be a continuous sequence of upper bound solutions involving mechanisms in which the conical portion for region EHR shrinks steadily to zero angle to give the exact mechanism as the limiting case for the exact $g(0)$ and $p = p_c$. Alternatively, as $p \to p_c$ from above, the complete exact solution for uniform pressure $p_c$ can be visualized for a typical octant as the limiting case of the exact solution for uniform pressure $p$ plus a line load along ER of total magnitude tending to zero as $p \to p_c$ with ER $\to 0$.

## 11. The exact solution for a clamped plate of any regular polygonal shape under uniform pressure

The preceding solution for the square plate is easily modified to cover the case of a plate of any regular polygonal shape. Thus the qualitative description of the exact solution in § 3 holds generally for a regular polygon of $n$ sides if figure 2 is interpreted as referring to a triangular region with the angle ACB equal to $\pi/n$; and the only changes in the earlier analysis are the substitution of $\pi/n$ for $\pi/4$ in equations (40), (43), (47), (51) and (55).




PHILOSOPHICAL TRANSACTIONS OF THE ROYAL SOCIETY A MATHEMATICAL, PHYSICAL & ENGINEERING SCIENCES

Numerical calculations for given $n$ can be carried out as for the square plate, but were limited in the present investigation to those necessary to find the collapse pressure $p_c$ for $n = 3$, 5 and 6, and to comparisons with upper bounds corresponding to the Mansfield and Wood patterns of figures 13 $a, b$ with angle ACB $= \pi/n$. Rounded results for the collapse pressure when $n = 3$, 4, 5 and 6 are given in Table 2 where $a =$ AC is the radius of the inscribed circle of the polygon.

Table 2 shows that the upper bounds become increasingly accurate as $n$ increases and that the Mansfield upper bound is especially close to the exact collapse pressure. The Mansfield–Morley upper bound (figure 13 $c$) would be even closer, but as indicated in table 1 for the square plate, the gain in accuracy would be very slight.

Salient dimensions of the moment net (figure 2 with angle ACB $= \pi/n$) were necessarily found in evaluating the exact collapse pressure. These indicated that for $n = 3$, 4, 5, 6, the deforming part of the plate bounded by ADE (figure 2) in the octant, extends nearer to the corner B for the exact solution than for either upper bound solution. However, the extension is very small in the comparison with the Mansfield mechanism since, expressed as a fraction of AC, the normal gap between the exact and Mansfield arcs DE is only about 0.01 for $n = 3$ and decreases with increasing $n$ to about 0.0004 for $n = 6$.

TABLE 2. VALUES OF $p_c a^2/m_0$ FOR CLAMPED PLATES OF REGULAR POLYGONAL SHAPE UNDER UNIFORM PRESSURE (VALUES IN PARENTHESES ARE PERCENTAGE OVERESTIMATES FOR UPPER BOUND SOLUTIONS)

| number of sides | exact solution | Mansfield upper bound | Wood upper bound |
|---|---|---|---|
| 3 | 9.6096 | 9.6568 (0.49%) | 9.9994 (4.1%) |
| 4 | 10.7128 | 10.7237 (0.10%) | 10.9630 (2.3%) |
| 5 | 11.1899 | 11.1937 (0.03%) | 11.3582 (1.5%) |
| 6 | 11.4421 | 11.4438 (0.01%) | 11.5619 (1.0%) |

## 12. ON WOOD'S ARGUMENTS CONCERNING THE NON-EXISTENCE OF EXACT SOLUTIONS IN LIMIT ANALYSIS FOR ISOTROPIC HOMOGENEOUS PLATES OBEYING THE SQUARE YIELD CRITERION

In his examination of the problem of the square clamped plate under distributed load, Wood (1969) emphasized the difficulty of satisfying all the necessary continuity conditions across a junction between a parabolic and a hyperbolic field; and he argued correctly that this is not possible when the junction is a hogging trajectory. But the case of a junction which is not a principal moment trajectory, as in the present solution, was dismissed by Wood on the grounds that 'mere inspection shows that shear could not be transmitted' and that 'radially increasing negative moments in the fan encounter constant negative moments in the surround, which is impossible'. The validity of these statements was questioned by Braestrup (1970) and in reply, Wood (1970) conceded that a junction of this type would enable all continuity conditions to be satisfied, but he commented that it would involve a sudden change in the curvature of the trajectories which he considered 'highly unlikely'. Such discontinuities in the curvature of the trajectories occur on the junction AFE (figure 2) in the present solution and do not violate any necessary stress or kinematic conditions; they seem likely to be a frequent feature of exact solutions. Secondly, in his reply to Braestrup, Wood argued that in any case a discontinuity of shear will occur across the junction where it crosses a diagonal of symmetry. But his argument involves

an implicit assumption that the junction is a curve of continuous slope and will coincide in direction with a hogging trajectory where it crosses a diagonal of symmetry. This is not necessary; thus in the present solution, the hogging trajectory DE (figure 2) is orthogonal to the diagonal at E, whereas the junction AFE intersects the diagonal at an angle of about 64°; but symmetry is maintained with the junction curve for the whole plate having corners on the diagonals. However, it is true in the present solution that if $r$ denotes a polar coordinate of origin H on the diagonal, there is a discontinuity at E between the value of the shear component $q_r$ in the parabolic field above E and its value in the corner hyperbolic field below E. But this is a discontinuity between the values of a shear force *per unit length* in regions which join only at a *single point* E and there is no violation of equilibrium.

We turn next to the question of whether the existence of an exact solution is likely to depend on the shape of the plate, as propounded by Wood (1965) in his original tentative hypothesis. Here we restrict comment to practical shapes of plate with piecewise smooth boundaries and to the common case where the two boundary conditions along any edge are (*a*) either the normal slope is zero or there is a given distribution of normal moment along the edge, and (*b*) either the deflexion is zero or there is a given distribution of the Kelvin–Tait shear reaction along the edge. For such conditions, no reason is known for expecting difficulties associated with the shape of the plate. Moreover, we note that an exact solution in limit analysis can be relatively insensitive to the precise shape of the plate since an exact mechanism is not required, *a priori*, to extend to all parts of the edge; and in undeflected regions the exact solution has only to satisfy the relatively unrestrictive condition of a statically admissible field. Such insensitivity is especially likely for clamped edges as illustrated in the extreme case by the well-known solution for a point load on a clamped plate where the same conical mechanism and radial stress field gives an exact solution for any shape of plate. A second example is the present solution for a clamped square plate under uniform pressure. Thus at a typical corner, there is an undeflected portion consisting of DEB (figure 2) and of D′EB in the adjacent octant, where D′E is the reflexion of DE in the diagonal CB. The present solution remains exact if the edge portions DB, D′B are replaced by a clamped edge along any curve joining D to D′ and lying within the area of existence of the field (59) for $v \geqslant 0$ (defining $F(u) = F(-u)$ to cover $u < 0$ in the adjacent octant). This area extends from DED′ to infinity in the direction EB with a non-dimensional half-width, on either side of EB and measured normal to EB, which increases from about 0.625 at D to unity at an infinite distance along EB produced.

Wood (1969) introduced the related question of the existence of exact solutions for elastic–plastic plates. In particular, he emphasized an observation by Kemp (1967) regarding the difficulty of satisfying all boundary conditions in a method proposed by Parkhill (1966) for finding an elastic–plastic stress field at the collapse load. The particular problem examined by Parkhill was that of a square plate, simply supported on all edges and subjected to uniform pressure. The exact solution for the corresponding problem in limit analysis, with yield governed by the square yield criterion, was known; it involves a mechanism of pyramid shape with yielding only on the diagonals, and Prager (1952) had given an associated statically admissible stress field. Parkhill assumed that the stress field at collapse for an elastic–plastic plate would be a purely elastic field in the triangular regions between the diagonals, and he claimed to have found a satisfactory solution numerically. Later, Wood (1971) pointed out that Parkhill had not checked that his solution satisfied the symmetry condition of zero shear on the diagonals, and on re-examining the problem numerically, Wood found that all the necessary continuity conditions on the





PHILOSOPHICAL TRANSACTIONS OF THE ROYAL SOCIETY A MATHEMATICAL, PHYSICAL & ENGINEERING SCIENCES

diagonals could not be simultaneously satisfied by an elastic stress field in the triangular regions bounded by the sides and the diagonals. This seems correct, but Wood then concluded in particular that 'Even in the case where an "exact" rigid–plastic stress field and mechanism are known, it is impossible to establish a corresponding elastic–plastic stress field *by present-day rules of limit analysis*' (italics as in Wood's paper). This conclusion is unjustified; there is no rule of limit analysis which requires that an elastic stress field should exist throughout a rigid region of a mechanism. Instead, limit analysis imposes the infinitely less restrictive condition that the field in a rigid region should be statically admissible. Nor, in *elastic–plastic* plate theory, is there any reason to require that, at the collapse load, an exact solution must lead to a purely elastic stress field throughout any region which is rigid in the corresponding rigid–plastic mechanism. Thus in Parkhill's problem, it is to be expected that a correct solution for an elastic–plastic plate will exhibit plastic yielding over some areas of the triangular regions at the collapse load. It is of course possible that there will be some purely elastic regions in an elastic–plastic plate at the collapse load, e.g. near the centre of the sides in Parkhill's problem. However, the junction between any such elastic region and an elastic–plastic region is not predetermined; hence its position will provide an extra parametric function for satisfying continuity conditions across the junction, in an analogous manner to the role of $v_j(u)$ in the problem of the present paper. Thus the investigation by Wood (1971) is not significant evidence for the non-existence of exact solutions; in this context, it simply shows that one particular form of stress field cannot exist at the collapse load in Parkhill's problem.

Summing up, the specific difficulties leading to Wood's doubts concerning the existence of exact solutions in the present field are now seen to be without foundation; in particular, there is no difficulty in satisfying the shear continuity condition across a junction between a parabolic and a hyperbolic stress field, and there is no evidence that the total number of necessary boundary conditions in a given problem will be larger than the number of available arbitrary functions such as $f_2(u)$, $g(u)$ and $v_j(u)$ in the present problem. Lastly, the scarcity of known exact solutions can be simply explained by their probable complexity even in apparently simple problems, as exemplified in the present problem and that of Fox (1972).

## 13. Conclusions

The present solution for a clamped plate of regular polygonal shape subjected to uniform pressure is an example of the possible complexity of exact solutions in limit analysis for plates even when the loading and edge conditions are apparently simple. Because of such complexity, known exact solutions in this field are likely to remain scarce. However, a comparison of the present exact results and those of Fox (1972) with earlier upper bound solutions provides evidence that mechanisms much simpler than the exact mechanism can lead to upper bound estimates of the collapse load within about 4 % of the exact collapse load; this is certainly within the accuracy with which the present theory of limit analysis for plates can be regarded as representing actual conditions in reinforced concrete slabs under lateral loading.



PHILOSOPHICAL TRANSACTIONS OF THE ROYAL SOCIETY A MATHEMATICAL, PHYSICAL & ENGINEERING SCIENCES

## References


Braestrup, M. W. 1970 Contribution to the written discussion on a paper by Wood (1969, reference below). *Mag. Concr. Res.* **22**, 109–114.

Collins, I. F. 1971 On an analogy between plane strain and plate bending solutions in rigid/perfect plasticity theory. *Int. J. Solids Struct.* **7**, 1057–1073.

Fox, E. N. 1968 The existence of exact solutions in Limit Analysis for homogeneous isotropic plates of rigid perfectly–plastic material. *Engineering plasticity* (ed. J. Heyman & F. A. Leckie), pp. 147–181. Cambridge University Press.

Fox, E. N. 1972 Limit analysis for plates: a simple loading problem involving a complex exact solution. *Phil. Trans. R. Soc. Lond.* A **272**, 463–492.

Hopkins, H. G. 1957 On the plastic theory of plates. *Proc. R. Soc. Lond.* A **241**, 153–179.

Kemp, K. O. 1967 Contribution to the discussion on a paper by Parkhill (1966, reference below). *Mag. Concr. Res.* **19**, 119–120.

Mansfield, E. H. 1957 Studies in collapse analysis of rigid–plastic plates with a square yield diagram. *Proc. R. Soc. Lond.* A **241**, 311–338.

Morley, C. T. 1965 Ph.D. dissertation. Cambridge University.

Parkhill, D. L. 1966 The flexural behaviour of slabs at ultimate load. *Mag. Concr. Res.* **18**, 141–146.

Prager, W. 1952 Sectional address. *8th Int. Congr. appl. Mech.*, Istanbul 1952.

Weatherburn, C. E. 1930 *Differential geometry of three dimensions*, vol. II, chap. 4. Cambridge University Press.

Wood, R. H. 1961 *Plastic and elastic design of slabs and plates*, pp. 176–177. Thames and Hudson.

Wood, R. H. 1965 New techniques in nodal-force theory for slabs. M.C.R. special publication: *Recent developments in yield-line theory*, pp. 31–62. London: Cement and Concrete Association.

Wood, R. H. 1969 A partial failure of limit analysis for slabs, and the consequences for future research. *Mag. Concr. Res.* **21**, 79—90.

Wood, R. H. 1970 Reply to the discussion on a paper by Wood (1969). *Mag. Concr. Res.* **22**, 109–114.

Wood, R. H. 1971 The importance of shear in the yield criterion for the bending of slabs. *J. Strain Analysis* **6**, 13–19.


## Appendix A. Numerical methods used for the evaluation of the moment net and the mechanism

For a given $g(0)$, the governing equations for evaluating the hyperbolic net and the junction are (18)–(21), (43), (50)–(53) and, as stated in § 7, the calculations marched out from A in equal steps $\Delta u$ in $u$, while for each $u$, the value of $v$ was increased in equal steps $\Delta v = \Delta u$ starting from the edge $u+v=0$. After the first step in $u$, the range covered in $v$ extended beyond the junction so that junction values could be obtained by interpolation. Except for the first step in $u$ and the first step in $v$ for given $u$, the integrals in (19) and (21) were extended step by step with the use of a quadrature formula corresponding to a parabolic fit to the integrand at the current and two previous mesh points. The successive stages of the numerical procedure were first, all properties at A where $u=0$, $v=0$, were found from the governing equations. Secondly, for $u$ and $v$ both small, the equations were used to derive the terms up to the third degree in power series for net and junction properties, and these series were used to evaluate properties for the first step $u=\Delta u$; similarly, for all later $u$, leading terms of power series in $(u+v)$ were derived and used to find properties for the first mesh point $u+v=\Delta v$ away from the edge. Thirdly, to extend the solution by a step $\Delta u$ to a new current $u$, the procedure was (*a*) estimates of $h_2(u,v)$, $g(u)$ and $v_1(u)$ were obtained by extrapolation from the results for the preceding $u$; (*b*) $s_2(u,v)$, $f_2(u)$, $h_1(u,v)$, $s_1(u,v)$ and $\lambda(u,v)$ were successively obtained from equations (19), (52), (18), (19) and (21), with interpolation for junction values; (*c*) $\mathrm{d}v_1/\mathrm{d}u$ and $\mathrm{d}g/\mathrm{d}u$ were found from (50) and (51) and together with values of these derivatives for $u-\Delta u$, $u-2\Delta u$, were used in the parabolic quadrature formula to obtain revised estimates of the current $v_1(u)$ and $g(u)$, while (18) was used to obtain revised values of the current $h_2(u,v)$; (*d*) the stages (*b*) and (*c*) were iterated with rapid convergence

except when $\frac{1}{4}\pi - \lambda_j$ became small near the end E of the net. After iteration, the values of $x$ and $y$ at mesh points were found from (21) with interpolation for junction values.

We consider next the evaluation of $g(u)$ from (54) starting from $g = \sqrt{3}$ for $\psi = 0$ and with given values of $s_{1j}$ and $\psi$ corresponding to $u = u_E$ and $u = 1.53(-0.005)0$ for the smallest mesh size. The stages of the computation were first, the leading terms for $g$ as a power series in $\psi$ were derived and used to obtain $g(1.53)$ and $g(1.525)$. Then for subsequent steps: ($a$) an estimate of the new current $g(u)$ was found by extrapolation and used to evaluate the integrand of (54); ($b$) the integration over the current interval in $\psi$ was performed by a parabolic quadrature formula; ($c$) the resulting cubic equation for $g$ was solved to give a revised value for the current $g(u)$ and hence for the current integrand of (54); ($d$) the stages ($b$) and ($c$) were iterated with rapid convergence at all steps.

The governing equations for the mechanism involve net properties, but excessive storage would have been required if the ncesssary net data at all mesh points had been found and stored prior to the evaluation of the mechanism. Instead, in the final forward evaluation of the net, only the basic data $f_2(u)$, $g(u)$, $v_j(u)$ together with data on the junction and on and near DE and DF were stored for use as input to the mechanism computations. There was then no difficulty in using (18), (19), (21), (5) and (64) to compute net properties by marching out from DE in DEF and from DF in ADF during the mechanism computations. Some input net data were not needed for this recalculation of net properties, but served instead as checks on the accuracy of the recalculations.

The mesh used for the computation of the mechanism properties in AFEDA (figure 2) consisted of the intersections of ($a$) the trajectories $u = 0.01(-0.005)1.53$ and DF with ($b$) the boundary ADE and the trajectories $v = v_j(u)$ corresponding to the preceding values of $u$. This enabled the boundary conditions to be used directly at mesh points. Integrations over steps in $u$ and $v$ were performed by a parabolic quadrature formula except for certain steps adjacent to boundaries where the trapezium rule was used.

For the numerical evaluation of $\zeta_u$, $\zeta_v$ in DEF (figure 2), equations (70), (71) and (75) were expressed in the integral equation forms

$$\zeta_u(u, v) = \zeta_u(u, v - \Delta v) + \int_{v-\Delta v}^{v} \mu_1 \zeta_v \, dv, \tag{A 1}$$

where the integration is along a trajectory $u$ = constant, and

$$\zeta_v = -\int_{u}^{u_j(v)} \mu_2 \zeta_u \, du, \tag{A 2}$$

where the integration is along a trajectory $v$ = constant meeting the junction AFE at $u = u_j(v)$. Now on DE, where $v = v_E$, the values of $\zeta_u$ are given by (74) and $\zeta_v$ then follows from (A 2). The computations of $\zeta_u$, $\zeta_v$ then marched out from DE with steps in $v$ as the outer loop. At each step in $v$, after first extrapolating $\zeta_u$ to the new value of $v$ at each mesh point, equations (A 2) and (A 1) were used successively in a rapidly convergent iteration process to obtain the final values of $\zeta_u$ and $\zeta_v$ (no iteration was needed on the junction where $\zeta_v = 0$).

Having found $\zeta_u$, $\zeta_v$, there are alternative methods for finding the slopes depending on the fact that equations (62), (63), (68) and (69) are not independent when $\zeta_u$, $\zeta_v$ satisfy (70) and (71). For the present solution, iteration was avoided by noting that equations (63), (69) and (73), with use of $\mu_2 = \partial\lambda/\partial v$ from (5) and (64), can be solved explicitly in terms of $\zeta_v$ to give

$$\left.\begin{aligned} \xi &= (1 - C_1)\sin\lambda' + D_1 \cos\lambda', \\ \eta &= (1 - C_1)\cos\lambda' - D_1 \sin\lambda', \end{aligned}\right\} \tag{A 3}$$

where $$C_1 = \int_{v_E}^{v} \zeta_v \cos\lambda' \, dv, \quad D_1 = \int_{v_E}^{v} \zeta_v \sin\lambda' \, dv, \tag{A 4}$$

and the integrals are along a trajectory $u$ = constant with $\lambda'$ equal to the change in net angle on this trajectory starting from $\lambda' = 0$ on DE.

For the numerical evaluation of $\zeta_u$, $\zeta_v$ in ADF (figure 2), the equations (70), (79) and (71) were expressed in the integral equation forms

$$\zeta_u = \int_{-u}^{v} \mu_1 \zeta_v \, dv, \tag{A 5}$$

where the integration is along a trajectory $u$ = constant, and

$$\zeta_v(u, v) = \zeta_v(u + \Delta u, v) - \int_{u}^{u+\Delta u} \mu_2 \zeta_u \, du, \tag{A 6}$$

where the integration is along a trajectory $v$ = constant.

Now the values of $\zeta_v$ on DF as defined in (81) were known from the calculations for the region DEF, and the values of $\zeta_u$ on DF were then found from (A 5). The computations then marched out from DF with steps in decreasing $u$ as the outer loop. At each new value of $u$, the mesh points on the edge AD and the junction AF were treated separately from the intermediate mesh points. At the edge mesh point, $\zeta_u = 0$ from (79) and then $\zeta_v$ was found from (A 6); though as the edge mesh point does not lie on a trajectory $v = v_j(u)$ corresponding to previous mesh points, this involved interpolation for the preceding value of $u$ to find the values of $\mu_2\zeta_u$ and $\zeta_v$ on the trajectory $v$ = constant passing through the new edge mesh point. For the intermediate mesh points, first estimates of $\zeta_v$ were obtained by extrapolation and then equations (A 5) and (A 6) were used successively in a rapidly convergent iteration process. Finally, the junction mesh point is special as the trajectory $v = v_j(u)$ through this point lies outside the mesh for the preceding values of $u$. However, $\zeta_v = 0$ from (75) at this point and $\zeta_u$ then follows from (A 5).

The edge slope on AD was found from (80), while the slopes at other mesh points were computed from the following solution of equations (63), (69) and (78)

$$\left.\begin{aligned} \xi &= [\eta(u, -u) - C_2] \sin\lambda + D_2 \cos\lambda, \\ \eta &= [\eta(u, -u) - C_2] \cos\lambda - D_2 \sin\lambda, \end{aligned}\right\} \tag{A 7}$$

where $$C_2 = \int_{-u}^{v} \zeta_v \cos\lambda \, dv, \quad D_2 = \int_{-u}^{v} \zeta_v \sin\lambda \, dv, \tag{A 8}$$

with integrations along a trajectory $u$ = constant.

In both DEF and ADF, the deflexion $w$ was found by integrating $h_2\eta$ with respect to $v$ along trajectories $u$ = constant, starting from $w = 0$ on ADE. Also, both for intrinsic interest and as an overall check on the mechanism calculations, the energy dissipation in the mechanism for an octant of the plate was computed and compared with the computed value of the work done by the pressure, noting that contributions from the developable surface are easily expressed in terms of integrals of mechanism properties along the junction AFE. The agreement was very satisfactory with a fractional error of order $10^{-8}$.



PHILOSOPHICAL TRANSACTIONS OF THE ROYAL SOCIETY A MATHEMATICAL, PHYSICAL & ENGINEERING SCIENCES

## Appendix B. The behaviour of $\zeta_u$, $\zeta_v$ for small values of $u$

Figure B 1 shows the region ADF (figure 2) in a plane of coordinates $(u, v)$; thus AD is the line $u+v=0$, FD is the line $u=-v_{\mathrm{E}}$, and AF is the curve $v=v_{\mathrm{j}}(u)$. The curvature of AF is too small to show in the figure, and AF is nearly coincident with the line $u+2v=0$ and lies slightly below it, so that

$$2v_{\mathrm{j}}(u)+u<0 \quad \text{for} \quad u>0 \quad \text{on AF}, \tag{B 1}$$

and if we let the inverse relation on AF be $u=u_{\mathrm{j}}(v)$, then

$$-v<u_{\mathrm{j}}(v)<-2v \quad \text{for} \quad u>0 \quad \text{on AF}. \tag{B 2}$$

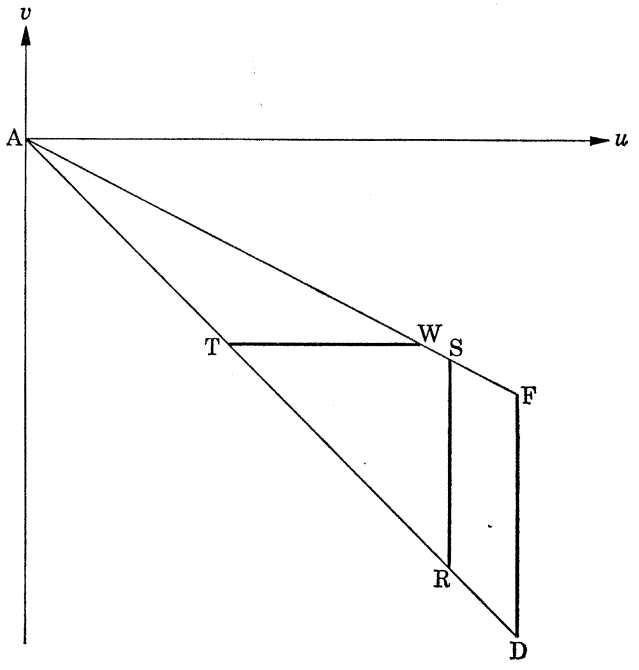


Figure B 1. Region ADF in $(u, v)$ plane.

Now, as discussed in § 7, $\zeta_u \geqslant 0$, $\zeta_v \leqslant 0$ in ADF with $\zeta_u=0$ on AD and $\zeta_v=0$ on AF, and then from (65), (70) and (71) it follows that $\zeta_u$ is a maximum on AF for given $u$, and that $-\zeta_v$ is a maximum on AD for given $v$. It suffices to consider these maximum values for which the numerical results indicate that $\zeta_u$, $-\zeta_v$ decrease steadily on AF, AD respectively as $u$ decreases. We note also that the maximum values of $\mu_2$ and $-\mu_1$ occur at A where each is equal to 1.15..., so that certainly

$$0<\mu_2, -\mu_1<2 \tag{B 3}$$

at all points in ADF.

In figure 16, RS is any typical line $u=u_0$ (say) in ADF and TW is the associated line $v=-\frac{1}{2}u_0$ and we note that W lies above S on AF by virtue of equation (B 1). Let the value of $-\zeta_v$ at R be $f(u_0)$; then from the above properties, $f(u_0)$ is the maximum value of $-\zeta_v$ in ARS so that

$$0 \leqslant -\zeta_v \leqslant f(u_0) \quad \text{for} \quad 0<u \leqslant u_0. \tag{B 4}$$

The value of $-\zeta_v$ at T is then $f(\frac{1}{2}u_0)$ and by integrating (71) along TW and using (75), we find

$$f(\tfrac{1}{2}u_0)=\int_{\frac{1}{2}u_0}^{u_j(v)} \mu_2 \zeta_u \, \mathrm{d}u, \quad (v=-\tfrac{1}{2}u_0). \tag{B 5}$$

Also, the value of $\zeta_u$ at any point $(u, v)$ in ARS is given by (A 5), whence using (B 3) and (B 4) we obtain

$$0 \leqslant \zeta_u \leqslant 2(u+v)f(u_0) \quad \text{for} \quad 0 < u \leqslant u_0, \tag{B 6}$$

which holds in particular for the values of $\zeta_u$ in (B 5). Then from (B 5), (B 3) and (B 6) we find

$$0 < f(\tfrac{1}{2}u_0) < 2f(u_0)\,[u_1(-\tfrac{1}{2}u_0) - \tfrac{1}{2}u_0]^2. \tag{B 7}$$

But from (B 2), $\frac{1}{2}u_0 < u_1(-\frac{1}{2}u_0) < u_0$, whence the inequality

$$0 < f(\tfrac{1}{2}u_0) < 0.5u_0^2 f(u_0) \tag{B 8}$$

holds for any $u_0 > 0$ in ADF, and in particular for $u_0$ small. Thus by halving the range of $u$, the maximum value of $-\zeta_v$ is reduced by a factor which tends to zero as $u \to 0$ at A. In contrast, if $-\zeta_v$ behaved predominantly like a finite power $u^m$ for small $u$ on AD, the effect of halving the range of $u$ would be a reduction by a constant factor $\frac{1}{2}^m$ in the limit $u \to 0$. Thus the maximum value of $-\zeta_v$ tends to zero faster than any finite power of $u$ as $u \to 0$, and $\zeta_v$ is not analytic at A. Finally from (B 6), for a given range of small $u$, the maximum value of $\zeta_u$ is of smaller order than the maximum value of $-\zeta_v$, whence $\zeta_u$ is also not analytic at A.